UNIVERSITY OF IOANNINA
SCHOOL OF SCIENCES
DEPARTMENT OF PHYSICS

Neutron capture cross section measurements by the activation method at the n_TOF NEAR station

MARIA-ELISSO STAMATI

PhD THESIS

IOANNINA 2025

ΠΑΝΕΠΙΣΤΗΜΙΟ ΙΩΑΝΝΙΝΩΝ
ΣΧΟΛΗ ΘΕΤΙΚΩΝ ΕΠΙΣΤΗΜΩΝ
ΤΜΗΜΑ ΦΥΣΙΚΗΣ

Μελέτη αντιδράσεων σύλληψης νετρονίων μέσω της τεχνικής της ενεργοποίησης στην πειραματική περιοχή **NEAR** των εγκαταστάσεων **n_TOF στο CERN**

ΜΑΡΙΑ-ΕΛΙΣΣΩ ΣΤΑΜΑΤΗ

ΔΙΔΑΚΤΟΡΙΚΗ ΔΙΑΤΡΙΒΗ

ΙΩΑΝΝΙΝΑ 2025

PhD committee

Three-member PhD advisory committee

- N. Patronis (Supervisor), Professor, Physics Department, University of Ioannina, Greece
- M. Kokkoris, Professor, School of Applied Mathematical and Physical Sciences, National Technical University of Athens, Greece
- M. Diakaki, Assistant Professor, School of Applied Mathematical and Physical Sciences, National Technical University of Athens, Greece

Seven-member PhD examining committee

- N. Patronis (Supervisor), Professor, Physics Department, University of Ioannina, Greece
- M. Kokkoris, Professor, School of Applied Mathematical and Physical Sciences, National Technical University of Athens, Greece
- M. Diakaki, Assistant Professor, School of Applied Mathematical and Physical Sciences, National Technical University of Athens, Greece
- S. Cohen, Professor, Physics Department, University of Ioannina, Greece
- J. Strologas, Assistant Professor, Physics Department, University of Ioannina, Greece
- V. Foteinou Assistant Professor, Physics Department, University of Ioannina, Greece
- M. Axiotis, Researcher, Institute of Nuclear and Particle Physics, NCSR Demokritos, Greece

But it was all right, everything was all right, the struggle was finished.

Acknowledgements

This work could not have been completed without the help and support of many people, all of whom I wish to name and wholeheartedly thank here:

Nikolaos Patronis, the academic supervisor of this thesis, for his guidance and patient explanations, for closely following all the steps of this work and dedicating as much time as needed to brainstorming and discussions until all the problems were one by one solved. Through this collaboration I learnt a lot and I became more creative with my work, something for which I am grateful.

The members of my advisor committee, **Maria Diakaki** for her contribution to this work, not only in the form of scientific advice but also of transmission of some much needed optimism and positive thoughts and **Michael Kokkoris**, the third member of my Advisor Committee, for his help and critical reading of this manuscript.

Augusto Ceccucci, my CERN Supervisor without whom my stay at CERN would not have been possible. I also thank him for finding time in his busy schedule to discuss my project and share his insight regarding the research world, always with a smile.

Alice Manna, the co-spokesperson of this experiment, for helping with the preparation of every aspect of it. **Alberto Mengoni**, **Cristian Massimi** and **Nicola Colonna** for setting this project in motion, their work on the proposal of the measurements and their feedback during all steps of my work. Special thanks to Alberto for all his help with various calculations that he performed or patiently explained to me.

Ulli Koester for his support, as he fast and efficiently provided us with the Zr sample we needed, helping with the best encapsulation of the Zr and Ge samples, as well as giving valuable insights before and during analysis procedure.

Claudia Lederer-Woods, for providing us with needed material such as precious $^{76}GeO_2$ powder as well as a new digitizer.

Simon Stegemann and **Edgar Miguel Sobral dos Reis** as there would be no pellet samples without their willingness to answer an almost stranger's email and agree to offer their equipment and their help.

Agatino Musumarra for wholeheartedly offering his help with setting

up a beta-spectrometer needed for some of the measurements and even flying to CERN to work on it during a holiday weekend. His help was much needed and his presence very much appreciated.

Oliver Aberle, **Oscar Fjeld**, **Ana-Paula Bernardes**, **Dominika Senajova** for making this practically possible. Specific shout-out to Oscar, for always transmitting incredible amounts of optimism even when I was panic-calling him to fix something lost in PhD chaos.

Un grand "merci" á **Jean-François Gruber** car, grâce á lui, beaucoup de bureaucratie et de nombreuses interventions sont devenues sûres et agréables. Merci d'être toujour calme et joyeux et d'avoir un Geiger-Muller.

The members of the local (or not so local) team with whom we shared many moments of our working (and not only) life:

My two office mates for adding some laughter to hard working days and always being there for me: **Simone Amaducci**, the person that was randomly assigned to share my office but proved to be a true friend (even if he kept hiding plastic spiders all over my things), and **Styliani (Stella) Goula**, later joining our office and finding her place next to me, literally and figuratively.

The permanent tenants of the n_TOF Control Room, sharing most of our working (and often non-working) days together: **Jose Antonio Pavón Rodríguez**, **Francisco García Infantes**, **Alice Manna**, **Adriá Casanovas Hoste**, **Michael (Michi) Bacak**. Special thanks to my "anonymous alcoholic" who lifted an incredible weight off off my shoulders, just by being there.

The long duration tenants of the Control Room, not there permanently but certainly left behind an empty spot: **Roberto Zarrella**, **Jorge Lerendegui Marco**, **Michele Spelta**, **Victor Alcayne Aicua**, **Victor Babiano Suarez**, **Pablo Perez Maroto**, **Pablo Torres Sanchez** as well as honorary mention **Massimo Barbagallo** who, unfortunately, was leaving the control room when I arrived.

Passers-by that didn't stay long but their stay was a pleasant break from our daily routine: **Ariel Tarifeño-Saldivia**, **Elizabeth Musacchio Gonzalez**, **Sotiris Chasapoglou**, **Veatriki Michalopoulou**. Special thanks to Veatriki as everytime she visited I learnt something new and overcame some analysis problem that was holding me back.

My University group for their help in scientific as well as personal matters, and for always having my back (just to talk or to send me cellulose): **Maria Peoviti**, **Efstathia (Effie) Georgali**, **Zinovia (Zina) Eleme**,

Styliani Goula, **Eleni Vagena**. Special thanks to Eleni Vagena for all her Geant4 input.

Andreas Tsiganis, although not directly working with him on this thesis, for always answering any question I had for him with wisdom and humour. I am also endlessly grateful to him because he was the one to think that I moved alone to this new demanding place and set the "local team" gears in motion.

Friends for infinite support with work and life in a foreign place: **Nikos Charitonidis** and **Spyridoula Florou**, the "Local Team" that (and I quote) forbade me to ever feel alone and abandoned, and words are not enough to describe the oasis they provided me with, as well as **Athanasios (Thanos) Stamatopoulos** who was always virtually there until I managed to get settled literally and figuratively.

Friends back at home for managing to make my life a bit happier even from far away: **Maria Peoviti**, **Stavros Stragalis**, **Marialena Vossou**, **Niki Tsironi** as well as **Maria Efthymiou**, whose visit during a very turbulent time brought a much needed feeling of understanding and "home".

I would also like to acknowledge the crucial contribution of **Ms. Marianna Kefallinou** and **Dr. Aikaterini Nteli** to the successful completion of this thesis.

At this point, I owe a second thanks to **Jose**. Even if we couldn't continue our common life, I am grateful for the support he offered me during those two first difficult years of our stay at CERN.

Lastly, position of honour for my family, **Eleni Gotovou**, **Ioannis Stamatis**, **Dia Christoyiannis** and my "chosen" family **Jean-François** et **Grisou** for the infinite support and love that got me through. Σας ευχαριστώ και σας αγαπώ. Je vous remercie et je vous aime. Meow.

Abstract

The lightest elements that make up our universe were created in the Big Bang. Elements heavier than Li-7 are produced every day in the heart of stars. Elements are synthesised in different nuclear processes taking place in different life stages of stars. Among other particles produced during these reactions, neutrons are readily available in stars and their velocities follow a Maxwell-Boltzmann distribution, centered around the value that corresponds to the star's temperature. One of the most important nucleosynthesis processes is the s-process, consisting of neutron captures and subsequent decays. Astrophysical models can deduce the elemental ratios and model the chemical evolution of our universe, but in order to accurately do so, they need input from nuclear reaction studies, such as accurate cross section values for astrophysical processes. Since neutrons in stars follow a Maxwellian distribution, these cross sections are referred to as Maxwellian-averaged cross sections, or MACSs. MACSs can be calculated by folding point-wise cross section data with a Maxwellian distribution or can be directly measured, if a Maxwellian neutron beam is available.

The neutron time-of-flight facility (n_TOF) is CERN's neutron source. Based on a proton beam from the proton synchrotron (PS) impinging on a lead spallation target, n_TOF comprises three experimental areas, two at the end of long flight paths in order to perform measurements using the time-of-flight (TOF) technique, and one right next to the spallation target itself, benefiting from high neutron flux. This third experimental area, the "NEAR" station, could potentially be used to perform integral MACS measurements on cases that are too challenging to measure via TOF. A prerequisite to this is to filter the neutron energy distribution into a Maxwellian one. This work is a feasibility study of such a filtering technique.

In order to shape the neutron energy distribution, filters made of B_4C, enriched in B-10 and thus highly interacting with low energy neutrons, were used. To test the shape results, neutron capture reactions of already known point-wise cross sections and MACS were measured. The methodology for these measurements was the activation technique, which consists of two steps: Irradiating the sample and afterwards measuring its induced activity. We can then deduce the number of nuclei of interest that was produced during the irradiation. This number is related to the cross section of the reaction for this specific shape of neutron flux.

By comparing the experimental results with the ideal-case results we would have gotten if we had had a perfect Maxwellian beam, we can quantify the quality of the shaping technique used in this study and make inferences as well as future suggestions.

The conclusions of this work can be summarised in the following two points:

- MACS can be measured at n_TOF only within a factor 2-3. This is not a high accuracy measurement, it can however be useful in cases where the MACS is completely unknown, or deduced with a large uncertainty.

- Thicker filters lead to smaller differences between experimental and ideal conditions. It should be noted though that increasing the thickness of the filters too much can have the opposite effect, as they then start to interfere too much and lead to further scattering or background issues.

- The experimental conditions can be significantly improved by the installation of a moderating system that will further shape the beam by interacting with the higher-energy neutrons, in addition to the filter that can absorb low energy ones.

Εκτεταμένη περίληψη

Πυρηνική αστροφυσική

Η πυρηνική αστροφυσική είναι ο τομέας της φυσικής που συνδυάζει παρατηρήσεις από την αστροφυσική με μοντέλα πυρηνικών αντιδράσεων με στόχο την καλύτερη κατανόηση της παραγωγής των στοιχείων στο σύμπαν καθώς και τη χημική εξέλιξή του.

Τα πιο ελαφρά στοιχεία του περιοδικού πίνακα, το υδρογόνο και το ήλιο, δημιουργήθηκαν κατά τη Μεγάλη Έκρηξη ενώ τα βαρύτερα στοιχεία από το 7Li παράγονται στα αστέρια. Ένας αστέρας δημιουργείται από την κατάρρευση αερίων στο σύμπαν. Το αέριο συμπυκνώνεται, τα άτομά του έλκονται όλο και ισχυρότερα και η θερμοκρασία ανεβαίνει. Έπειτα από κάποια συγκεκριμένη θερμοκρασία, η ενέργεια των ατόμων του υδρογόνου είναι υψηλότερη από το φράγμα Κουλόμπ και μπορούν πλέον να ξεκινήσουν αντιδράσεις σύντηξης. Η κατάρρευση σταματά προσωρινά καθώς η δύναμη της βαρύτητας εξισορροπείται από την παραγωγή ενέργειας μέσω σύντηξης και ήλιο ξεκινά να παράγεται.

Όταν το διαθέσιμο υδρογόνο στον πυρήνα του άστρου εξαντληθεί, η κατάρρευση ξαναξεκινά και ο αστέρας μετατρέπεται σε ερυθρό γίγαντα, ακτινοβολεί ενέργεια και η θερμοκρασία του πυρήνα του εξακολουθεί να αυξάνεται μέχρις ότου καταστεί δυνατή η σύντηξη του ηλίου, οπότε η κατάρρευση σταματά και πάλι.

Ο αστέρας θα συνεχίσει αυτή την ακολουθία περιόδων κατάρρευσης και ισορροπίας, με τα διαφορετικά στοιχεία να παράγονται μέσω διαφορετικών αντιδράσεων που ξεκινούν στα αντίστοιχα στάδια εξέλιξης. Κάθε αντίδραση που λαμβάνει χώρα μέσα στο άστρο δεν παράγει μόνο κάποιο βαρύτερο στοιχείο, αλλά πολλά ακόμα σωματίδια όπως ηλεκτρόνια, νετρίνα και άλλα. Μεταξύ αυτών βρίσκονται και τα νετρόνια, τα οποία παράγονται και κινούνται μέσα στο υλικό του αστέρα και, καθώς συγκρούονται με τα υπόλοιπα σωματίδια, σιγά σιγά αποκτούν ταχύτητες που αντιστοιχούν στη θερμοκρασία του άστρου. Η κατανομή των ταχυτήτων αυτών των νετρονίων είναι τότε μία κατανομή Maxwell-Boltzmann.

Καθώς τα νετρόνια αυτά κινούνται μέσα στο υλικό του αστέρα, κάποια στιγμή θα συλληφθούν από κάποιο άτομο. Η πιθανότητα να συμβεί αυτή η σύλληψη δίνεται από τη μέση ενεργό διατομή της συγκεκριμένης αντίδρασης για νετρόνια που ακολουθούν κατανομή Maxwell-Boltzmann αντίστοιχη της θερμοκρασίας του άστρου. Η τιμή αυτή ονομάζεται Maxwellian-averaged cross section (MACS) και αυτή η ορολογία θα χρησιμοποιείται στη συνέχεια αυτού του κειμένου.

Στόχος αυτής της μελέτης είναι να διερευνηθεί η δυνατότητα πραγματο-

Σχήμα 1: Η πειραματική περιοχή NEAR, ακριβώς μπροστά από τη θωράκιση του μολύβδινου στόχου.

ποίησης μετρήσεων MACS μέσω της τεχνικής της ενεργοποίησης στις εγκαταστάσεις n_TOF του CERN, και συγκεκριμένα στην πειραματική περιοχή NEAR.

Πειραματικές εγκαταστάσεις

Η εγκατάσταση n_TOF του CERN βασίζεται σε μία από τις ισχυρότερες πηγές ταχέων νετρονίων. Πρωτόνια από τον επιταχυντή PS συγκρούονται με στόχο μολύβδου οδηγώντας σε αντιδράσεις θρυμματισμού οι οποίες παράγουν διαφορετικά στοιχεία και σωματίδια, μεταξύ των οποίων νετρόνια. Για κάθε πρωτόνιο παράγονται περίπου 300 νετρόνια, κινούμενα προς όλες τις κατευθύνσεις. Από αυτά, ένα μικρό ποσοστό κατευθείνεται προς τις τρεις πειραματικές περιοχές της εγκατάστασης. Οι δύο από αυτές, οι EAR1 και EAR2, βρίσκονται μακρυά από το στόχο, 185 και 20 μέτρα αντίστοιχα, ώστε να επιτρέπουν μετρήσεις με την τεχνική time-of-flight (TOF), τεχνική που εκμεταλλεύται την καλή γνώση της απόστασης και του χρόνου πτήσης των νετρονίων για τον υπολογισμό της ενέργειάς τους. Η τρίτη πειραματική περιοχή των εγκαταστάσεων, ο σταθμός NEAR βρίσκεται κοντά στο στόχο, σε απόσταση μόλις 3 μέτρων, με σκοπό να εκμεταλλευτεί την πολύ υψηλή ροή νετρονίων εκεί. Οι πειραματικές διατάξεις τοποθετούνται σε αλουμινένια υποστηρικτική ράγα και ευθυγραμμίζονται με την αντίστοιχη οπή στη θωράκιση και την διάταξη του ευθυγραμμιστή της δέσμης (collimator). Η πειραματική περιοχή NEAR φαίνεται στο Σχήμα 1.

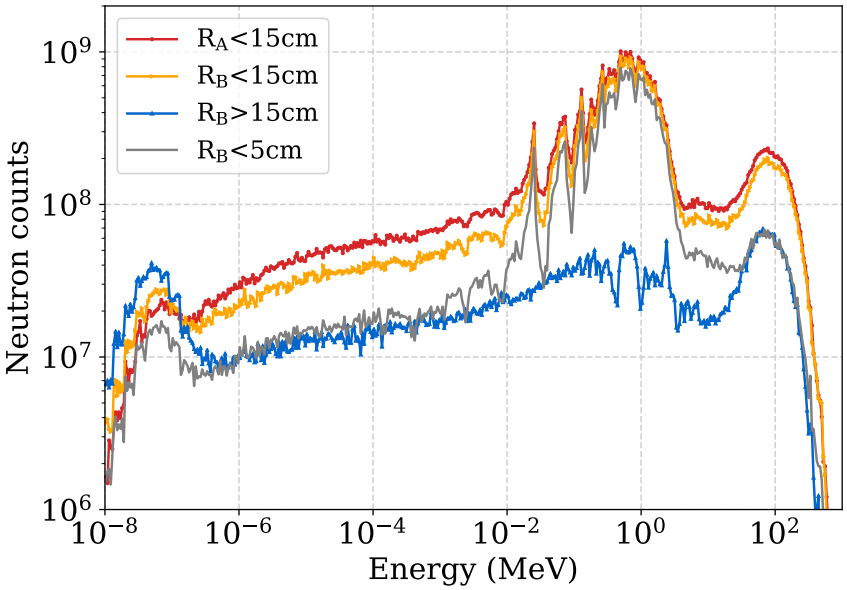

Σχήμα 2: Ενεργειακή κατανομή των νετρονίων στο σταθμό NEAR όπως υπολογίζεται από προσομοιώσεις. Τα διαφορετικά χρώματα αντιστοιχούν σε μικρότερες ή μεγαλύτερες επιφάνειες. Προσομοιώσεις και γράφημα: M. Cecchetto.

Μέθοδος και εξοπλισμός

Η ενεργειακή κατανομή των νετρονίων που φτάνουν στον πειραματικό σταθμό NEAR εκτείνεται από μερικά meV μέχρι την περιοχή των GeV, καθώς τα νετρόνια προέρχονται από αντιδράσεις θρυμματισμού στο στόχο. Αυτή η ενεργειακή κατανομή για διαφορετικές επιφάνειες κατά μήκος της δέσμης του πειραματικού σταθμού, όπως προέκυψε από εκτεταμένες προσομοιώσεις που πραγματοποιήθηκαν με τον κώδικα FLUKA δίνεται στο σχήμα 2. Οι προσομοιώσεις πραγματοποιήθηκαν από την ομάδα FLUKA του CERN/SY.

Όπως απεικονίζεται και στο σχήμα, η κατανομή των νετρονίων δεν ακολουθεί την κατανομή Maxwell-Boltzmann που θα θέλαμε για μετρήσεις αστροφυσικού ενδιαφέροντος. Αυτό όμως μπορεί να αλλάξει με τη χρήση κατάλληλων φίλτρων, τα οποία θα απορροφήσουν νετρόνια χαμηλής ενέργειας, μεταβάλλοντας έτσι το σχήμα της ενεργειακής κατανομής τους. Ένα υλικό κατάλληλο για τέτοια φίλτρα είναι το βόριο, εμπλουτισμένο στο ισότοπο βόριο-10. Για τη συγκεκριμένη μελέτη χρησιμοποιήθηκαν 4 φίλτρα βασισμένα στο βόριο-10, με διαφορετικά πάχη, ώστε να μελετηθούν διαφορετικές κατανομές και να διερευ-

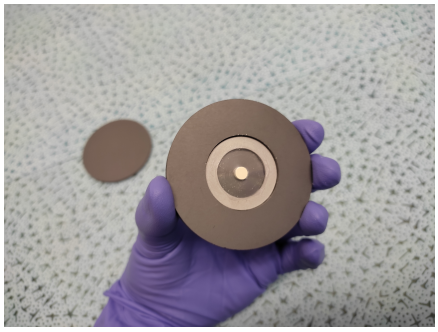

(α′) Δείγμα σε φίλτρο

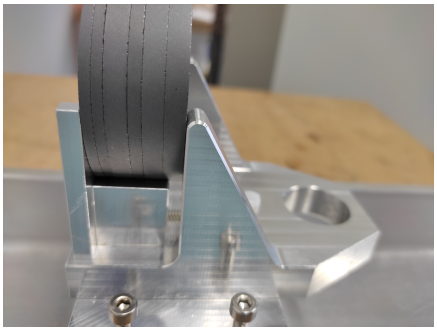

(β′) Πλήρης διάταξη

Σχήμα 3: Παράδειγμα πειραματικής διάταξης δείγματος - φίλτρου

Αντίδραση	**Προϊόν**	**Χρόνος ημιζωής**	**Ενέργεια ακτίνας γ [keV]**
140Ce(n,γ)	141Ce	32 ημέρες	145.4
76Ge(n,γ)	77Ge	11.2 ώρες	264.5
94Zr(n,γ)	95Zr	64 ημέρες	724.2
197Au(n,γ)	198Au	2.69 ημέρες	411

Πίνακας 1: Υπό μελέτη αντιδράσεις και βασικά χαρακτηριστικά τους: προϊόν της αντίδρασης, χρόνος ημιζωής του και χαρακτηριστική ακτίνα γ που μετρήθηκε.

νηθεί κατά πόσον μπορούν να οδηγήσουν σε μετρήσεις MACS . Αποφασίστηκε επίσης να μελετηθούν 4 αντιδράσεις που έχουν μελετηθεί ήδη με την τεχνική χρόνου πτήσης, με γνωστή MACS , ώστε να μπορεί να ποσοτικοποιηθεί η αποτελεσματικότητα ή μη των φίλτρων. Μαζί με το κάθε δείγμα τοποθετήθηκε και φύλλο χρυσού, δρώντας ως στόχος αναφοράς. Στο σχήμα 3 φαίνεται ένα δείγμα και τα φίλτρα που θα το περικυκλώσουν κατά την ακτινοβόληση ενώ στον πίνακα 1 αναγράφονται οι υπό μελέτη αντιδράσεις και τα βασικά χαρακτηριστικά τους.

Η μέθοδος που ακολουθήσαμε για αυτές τις μετρήσεις ήταν η τεχνική της ενεργοποίησης. Η τεχνική αυτή αποτελείται από δύο βήματα: την ακτινοβόληση ενός δείγματος και τη μετέπειτα μέτρηση της επαγόμενης ενεργότητας. Κατά την ακτινοβόληση λαμβάνει χώρα η υπό μελέτη αντίδραση ενώ η μέτρηση της επαγόμενης ενεργότητας οδηγεί στον υπολογισμό του αγνώστου μεγέθους που μπορεί να είναι η ενεργός διατομή της αντίδρασης, εάν η ροή κατά την ακτινοβόληση είναι γνωστή, ή το αντίστροφο.

Στην παρούσα μελέτη η μέτρηση της ενεργότητας πραγματοποιήθηκε με

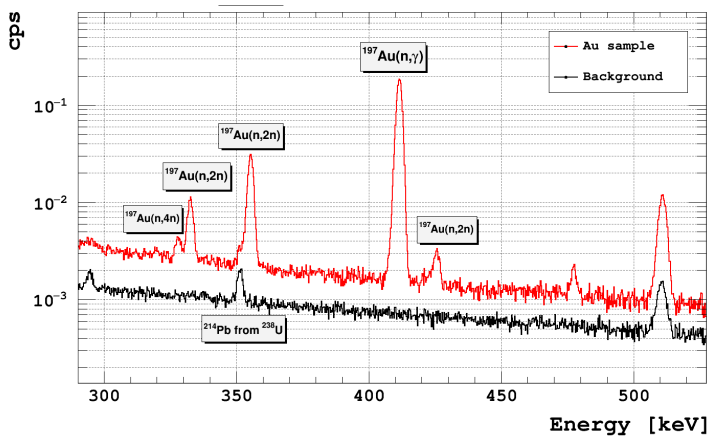

Σχήμα 4: Παράδειγμα φάσματος γ. Με κόκκινο: Φάσμα από δείγμα χρυσού. Με μαύρο: Φυσικό υπόβαθρο της μέτρησης, κανονικοποιημένο στον αντίστοιχο χρόνο.

ανιχνευτή γερμανίου υπερυψηλής καθαρότητας (HPGe). Επρόκειτο για έναν ανιχνευτή γερμανίου εγκατεστημένο σε υπόγειο χώρο και μέσα σε μολύβδινη θωράκιση πάχους 10 εκατοστών, ώστε να λειτουργεί στις καλύτερες δυνατές συνθήκες υποβάθρου. Πριν τη χρήση του για τις μετρήσεις, βαθμονομήθηκε με ραδιενεργές πηγές και με βάση αυτή τη βαθμονόμηση μοντελοποιήθηκε με τη βοήθεια του υπολογιστικού πακέτου GEANT4. Η διαδικασία αυτή ονομάζεται χαρακτηρισμός του ανιχνευτή και είναι απαραίτητη ώστε, στα επόμενα στάδια της μελέτης, να μπορεί να υπολογιστεί με ακρίβεια η ανιχνευτική του απόδοση.

Ανάλυση δεδομένων

Τα δεδομένα που έχουμε στο τέλος της μέτρησης της ενεργότητας είναι φάσματα-γ, όπως αυτά που απεικονίζονται στο σχήμα 4. Με βάση αυτά τα φάσματα μπορούμε να υπολογίσουμε τον αριθμό των πυρήνων που παρήχθησαν κατά την ακτινοβόληση. Αρχικά πρέπει να υπολογίσουμε τον αριθμό των γεγονότων που καταγράφηκαν στη φωτοκορυφή, καθώς αυτά αντιστοιχούν σε φωτόνια που εκπέμφθηκαν από το δείγμα κατά τη διάρκεια της μέτρησης, σταθμισμένα φυσικά με την ανιχνευτική απόδοση του συστήματός μας.

Αφότου προσδιορίσουμε τον αριθμό των γεγονότων από την ανάλυση των φασμάτων και πριν καταλήξουμε στον αριθμό των παραγόμενων πυρήνων, χρειάζεται να εφαρμόσουμε ορισμένες διορθώσεις:

- Διόρθωση για τους πυρήνες που παρήχθησαν κατά την ακτινοβόληση αλλά αποδιεγέρθηκαν επίσης κατά τη διάρκειά της, μη φτάνοντας έτσι στο στάδιο της μέτρησης: Υπολογίζεται με βάση τις πληροφορίες που έχουμε από βάσεις δεδομένων του CERN για την ακριβή ροή πρωτονίων στο στόχο μολύβδου (και άρα παραγωγής δέσμης νετρονίων) ανά τακτά χρονικά διαστήματα.

- Διόρθωση για τους πυρήνες που αποδιεγέρθηκαν στο διάστημα ανάμεσα στην ακτινοβόληση και τη μέτρηση: Υπολογίζεται με βάση το νόμο της εκθετικής αποδιέγερσης για το χρονικό διάστημα που μεσολάβησε.

- Διόρθωση για τους πυρήνες ενδιαφέροντος για αυτή τη μελέτη, που όμως παρήχθησαν από κάποια διαφορετική, ανταγωνιστική αντίδραση και όχι την αντίδραση που ενδιαφερόμαστε να μελετήσουμε: Υπολογίζεται λαμβάνοντας υπ΄όψιν την ροή νετρονίων στο δείγμα μας (μέσω προσομοιώσεων) και την ενεργό διατομή και των δύο αντιδράσεων, και υπολογίζοντας θεωρητικά το ποσοστό συμμετοχής της κάθε μίας στην παραγωγή του πυρήνα που μας ενδιαφέρει. Αυτή η διόρθωση προσδίδει ένα μεγάλο ποσοστό ¨αβεβαιότητας' στα δεδομένα μας, καθώς εξαρτάται σημαντικά από τη βιβλιοθήκη ή βάση δεδομένων από την οποία αντλούμε τα δεδομένα της ενεργού διατομής. Στη συγκεκριμένη εργασία χρησιμοποιήθηκαν διαφορετικές βιβλιοθήκες για τον υπολογισμό αυτής της διόρθωσης και στα τελικά αποτελέσματα χρησιμοποιήθηκε μία μέση τιμή, ενώ οι διαφορές ανάμεσα στα δεδομένα ενεργού διατομής λαμβάνονται υπ΄όψιν ως ένα είδος συστηματικής ¨αβεβαιότητας¨.

Αφότου εφαρμόσουμε όλους τους διορθωτικούς παράγοντες που απαιτούνται, καταλήγουμε στον αριθμό των πυρήνων που παρήχθησαν, μέγεθος άμεσα συνδεδεμένο με την ενεργό διατομή της αντίδρασης για τη συγκεκριμένη ενεργειακή κατανομή νετρονίων. Αυτή η ενεργός διατομή ονομάζεται Μέση φασματική ενεργός διατομή (Spectral-averaged cross section (SACS)) και, για να ποσοτικοποιήσουμε τα αποτελέσματα της μελέτης, πρέπει να συγκρίνουμε τον αριθμό αυτόν με τον ιδανικό αριθμό που θα είχαμε εάν η ενεργειακή κατανομή των νετρονίων ήταν μία τέλεια κατανομή Maxwell-Boltzmann, δηλαδή τη MACS. Για να αποφύγουμε τυχόν συστηματικά σφάλματα που μπορούν να υπονομεύσουν την ακρίβεια αυτής της μελέτης, υπολογίσαμε το λόγο των SACS δείγματος και στόχου αναφοράς και συγκρίναμε με τον αντίστοιχο λόγο των MACS.

Η σύγκριση αυτών των λόγων φαίνεται στο σχήμα 5. Το μεγάλο εύρος στα αποτελέσματα της προσομοίωσης (κυανό χρώμα) καθώς και τα αποτελέσματα των MACS (κίτρινο χρώμα) οφείλεται κυρίως στις διαφορές των βιβλιοθηκών

με δεδομένα ενεργού διατομής.

Τα συμπεράσματα από αυτό το σχήμα μπορούν να καταγραφούν ως εξής:

- Μεγαλύτερα πάχη φίλτρου οδηγούν σε πειραματικές τιμές (μωβ χρώμα) πιο κοντινές στις ιδανικές (κίτρινο χρώμα).

- Για υψηλής ακρίβειας υπολογισμούς MACS, δεν αρκεί μόνο η διαδικασία του φιλτραρίσματος της ροής ώστε να απομακρυνθούν τα νετρόνια χαμηλής ενέργειας. Αυτό φαίνεται από το γεγονός ότι τα πειραματικά δεδομένα (μωβ χρώμα) απέχουν από τα ιδανικά (κίτρινο χρώμα) κατά έναν παράγοντα 2-3. Παρ΄όλα αυτά, αυτή η ακρίβεια μπορεί να είναι ικανοποιητική για αντιδράσεις των οποίων η MACS δεν είναι γνωστή, ή είναι γνωστή με πολύ μεγάλη αβεβαιότητα.

Ένας τρόπος να βελτιωθεί η δυνατότητα μέτρησης MACS μέσω της τεχνικής της ενεργοποίησης στην πειραματική περιοχή NEAR του n_TOF είναι η επιπλέον εγκατάσταση ενός συστήματος moderator, με το οποίο θα αλληλεπιδρούν τα νετρόνια πιο υψηλής ενέργειας, ώστε να μεταβληθεί περαιτέρω το σχήμα της ενεργειακής κατανομής των νετρονίων, πλησιάζοντας το πιο κοντά στο ιδανικό.

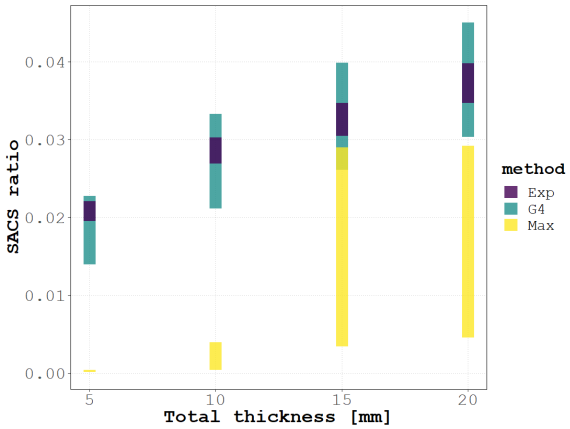

(α′) Ce sample

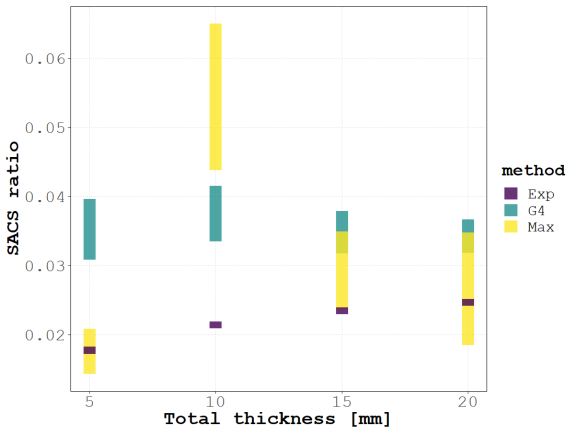

(β′) Ge sample

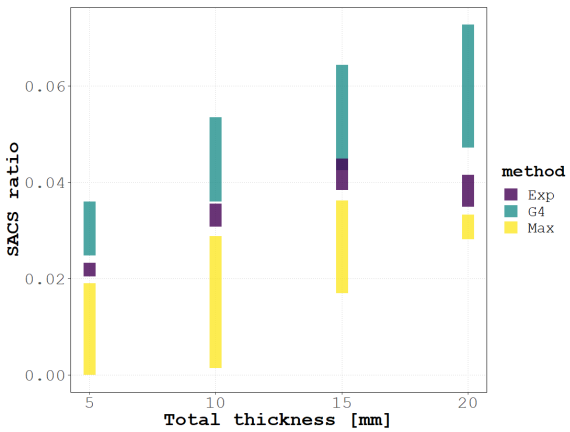

(γ′) Zr sample

Σχήμα 5: Σύγκριση μεταξύ λόγων πειραματικών SACS (μωβ), λόγων SACS υπολογισμένων με βάση προσομοιώσεις (κυανό) και λόγων MACS (κίτρινο).

Contents

1 Introduction

1.1 Nuclear Astrophysics

Nuclear astrophysics is the scientific field that combines nuclear physics and astrophysics. Based on astronomical observations and nuclear physics theories and models, it explores the processes of nucleosynthesis in stars, and the role of these processes in the distribution of elements and chemical evolution of the universe.

1.1.1 Stellar evolution

A star is created when interstellar gas collapses due to gravity. If the gravitational energy is larger than the thermal energy of the molecules and atoms of the gas cloud, then it becomes unstable and collapses. The density of the central region of the gas cloud increases and, if anisotropies exist, it can fragment into independent collapsing clouds leading to the creation of not only one but many stars. Sometimes, largely in the case of smaller clouds, the thermal pressure is enough to prevent gravitational collapse. In these cases, an external event such as a shock wave is needed to initiate the procedure.

Stars begin their life cycle containing mainly hydrogen, the most abundant element in the universe. As the gas cloud collapses, the kinetic energy of atoms increases, thus the temperature of the gas rises. After a while, the temperature is high enough for protons (hydrogen nuclei) to overcome Coulomb barriers and fusion reactions to start. The gravitational collapse is temporarily halted, as the star can produce enough energy through hydrogen fusion into helium, a process called "hydrogen burning" and which essentially constitutes the first stage of the life of a star. During this lengthy stage, the star doesn't change considerably in size, temperature or luminosity. In a Hertzsprung–Russell (H-R) diagram, a tool for categorising stars into evolutionary phases based on their luminosity and temperature, a star in the hydrogen burning phase would belong to the so-called "main sequence" region. The main sequence is a diagonal line containing as many as 80% of the stars on the diagram. The diagram is pictured in Fig. 6.

Eventually, the hydrogen in the core of the star will become exhausted and the core will predominantly consist of helium. The star will then resume its gravitational contraction, since it has run out of hydrogen fuel. This causes more energy to be generated at the core, igniting the surrounding hydrogen shell. Even as a star evolves off the main sequence, hydrogen burning remains an important energy source. At this stage, more energy can

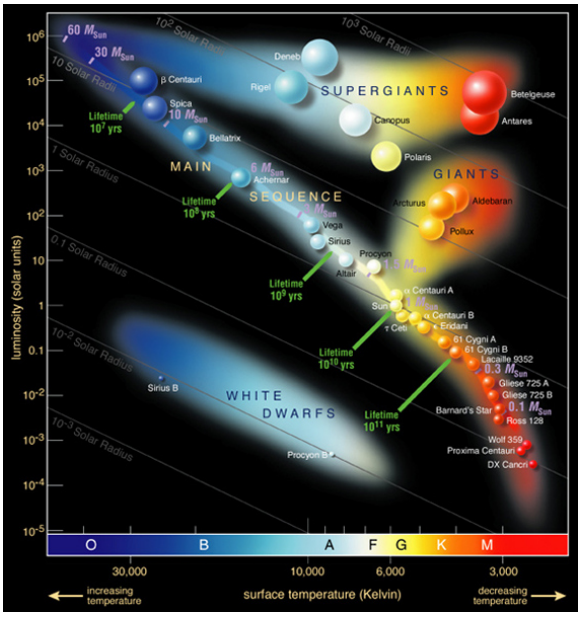

Figure 6: The Hertzsprung–Russell (H-R) diagram. Figure from the European Southern Observatory.

be radiated away at the star's surface, making its outer layers expand and cool down. The star is now moving upward in the H-R diagram, becoming brighter and redder, classified as a red giant. When the central temperature raises enough, helium burning begins. The helium burning reaction releases less energy than the hydrogen one, so more reactions, and thus more helium destruction, are needed to generate the same amount of energy. This is why the red giant neighbourhood of the H-R diagram is less crowded than the main sequence and the star's passage from it is faster than that of the main sequence. The length of the helium burning phase depends on the lifetime of the star and its future evolution. If the mass of the star is low, it will eventually eject its envelope and become a white ward, gradually cooling and fading away. If the star however has a mass higher than 1.4 times the mass of the sun, it will evolve more violently. Stars with moderate mass will end up as white dwarves after a nova mechanism, while in stars with higher masses, each burning product will become fuel for the next in between collapsing phases. Thus, after helium comes the carbon-oxygen burning. Each stage produces less energy than the previous one and energy losses increase. This successive chain reaches its end when the core consists

mainly of iron, the element with the highest binding energy per nucleon. Beyond iron, there is no energy gain through combining nuclei thus the star will inevitably collapse and explode as a supernova [1–4].

1.1.2 Stellar nucleosynthesis and the s-process

The lightest elements of the universe were produced in the Big Bang. The standard model of cosmology is quite successful in explaining those elements' abundances, which cannot be reproduced only by nucleosynthesis in stars. The only way to reproduce them is Big Bang nucleosynthesis, which has thus been used as a probe for early universe studies. Such studies are important as they provide limits and constraints in both particle physics and cosmology [5]. An example of that is the constraint in the number or light neutrino species as explained in [6].

Heavier elements are synthesised in the hearts of stars. The underlying nucleosynthesis processes depend on the star's size and evolution. Based on the distribution of masses of stars that are formed in the region around the Sun, it can be derived that [7]:

- 90% of stars are low in mass, specifically with a mass less than 0.8 solar masses
- Approximately 10% of stars have intermediate masses, with values between 0.8 and 8 solar masses.
- Less than 1% are characterised as massive, meaning they have a mass of more than 8 solar masses.

Most supernovae evolve from massive stars, main sequence stars with masses greater than 8 times the mass of our Sun. All these stars produce a collapsing iron core after their hydro-static evolution. In most cases, a central neutron star or black hole is created and the envelope is ejected after a shock wave. A considerable portion of the heaviest elements of the universe are synthesised in these violent processes [8].

Each low mass star enriches the interstellar medium with fewer new elements than a high mass star, however, collectively because of their number, low and intermediate stars (LIM) become more significant contributors [9]. One of the most important astrophysical processes responsible for nucleosynthesis in LIM stars is the s-process, comprising neutron capture events and subsequent beta decays. It is named slow process, as it takes place in environments with lower neutron fluxes and each element created by a neutron capture has enough time to decay before capturing another neutron.

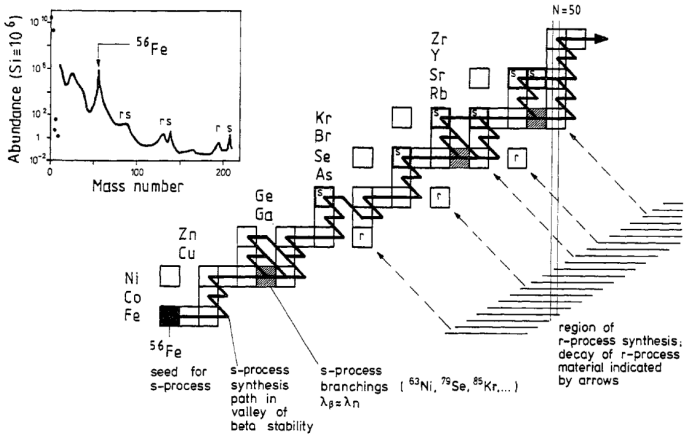

Figure 7: Path of the s-process after ^{56}Fe. Taken from [11]

The s-process path after ^{56}Fe can be seen in Fig. 7. More than half of the elements heavier than iron are produced through this process [10].

The majority of s-process elements is synthesised in LIM stars while they are in the asymptotic giant branch (AGB) phase of their evolution [12], as neutrons are much more easily released in that phase. During this phase, the star has exhausted the hydrogen and helium fuel in its core, causing it to expand and cool, becoming a large, luminous red giant. The AGB phase is characterized by two shells around the star's core where nuclear fusion occurs: an inner shell fusing helium into carbon and oxygen, and an outer shell fusing hydrogen into helium. A typical temperature for a star in this phase of its life is about 300 Million Kelvin, which corresponds to thermal neutrons of approximately 30 keV. The star experiences intense mass loss through strong stellar winds, creating a circumstellar envelope of gas and dust. Ultimately, stars in the AGB phase shed their outer layers, forming a planetary nebula, while the remaining core becomes a white dwarf.

The production of elements and their proportions by the s-process can be deduced using astrophysical models. These models highly depend on initial parameters such as star mass and metallicity and different approaches can yield different results (see [13]) [9]. Furthermore, abundance predictions are dependent on nuclear physics quantities, thus the uncertainties of the latter have a great impact on the former [14–16].

For a more detailed analysis of astrophysical observations and nuclear physics in nuclear astrophysics, see [11, 17, 18].

1.2 Maxwellian Averaged Cross-Sections

The probability of a nuclear reaction occurring between two nuclei depends on several parameters. It is affected by their relative velocities as well as the nuclear stucture of the involved isotopes, the type of reaction, etc. This probability is often expressed in terms of the "nuclear surface", or alternatively, as the number of reactions per intensity unit of incident particles. Inside stars, gas is in thermodynamic equilibrium, which leads all particle velocities to follow the Maxwell-Boltzmann law. This means that most particles have a velocity around a "most probable" value which depends on the star's temperature. The higher the temperature, the broader the distribution. At lower temperatures, the distribution is narrower with more particles having velocities closer to the average. Mathematically, we can say that the number of particles with velocity between v and $v + dv$ is

$$N(v)dv = N(\frac{m}{2\pi kT})^{3/2} exp(-\frac{mv^2}{2kT})dv \tag{1.1}$$

where:

- N – Number of particles in the system.
- m – Mass of a single particle.
- k – Boltzmann constant (1.38×10^{-23} J/K).
- T – Temperature of the system in Kelvin.
- v – Velocity of the particle.
- dv – Small velocity interval.

If the particles are charged, they need to overcome their Coulomb repulsion barrier in order to interact. Typically in stars, their energy will not be sufficiently high to overcome the Coulomb barrier, however, once in a while, they can approach enough thanks to the quantum tunneling effect, which enables nuclear reactions at low energies.

As the atomic mass of the interacting particles increases, however, so does the Coulomb barrier, making it more and more difficult for fusion to occur. For nuclei with atomic mass $A > 64$, fusion can only occur at temperatures of the order of 5-6 billion Kelvin [4]. Such temperatures favour photo-disintegration reactions and fusion cannot anymore explain the production of elements heavier than iron. These are produced by neutron captures, since neutrons do not have charge and thus Coulomb barrier to limit

their interactions. Contrary to that of fusion reactions, the general trend of the cross section of neutron capture reactions in that energy region is a decrease with energy as $\sigma \propto 1/\sqrt{E}$

Neutrons exist in stars thanks to reactions such as

$$^{13}C(\alpha, n)^{16}O$$

and

$$^{22}Ne(\alpha, n)^{25}Mg$$

and they, too, follow a Maxwellian distribution of velocities. When they interact with nuclei, for example when they are captured in the course of the s-process, the reaction rate depends on the velocity of both the neutron and the capturing nucleus. If we introduce the center-of-mass energy $E = \frac{1}{2}\mu v^2$, we can say about the reaction rate [1]:

$$< \sigma v >= (\frac{8}{\pi\mu})^{1/2} \frac{1}{(kT)^{3/2}} \int_0^\infty \sigma(E) E exp-(\frac{E}{kT}) dE \tag{1.2}$$

This equation describes the reaction rate at a given stellar temperature T. If the temperature changes, the reaction rate needs to be re-evaluated at the new temperature of interest.

The reaction rate per particle pair can be considered constant and thus

$$< \sigma v >= constant =< \sigma > v \tag{1.3}$$

This $< \sigma >$ is the Maxwellian-averaged cross section, known as MACS, the knowledge of which can help our understanding of the underlying nucleosynthesis processes, such as the s-process.

From the point of view of nuclear physics, MACS can be extracted in two ways:

i) Integral measurements: Irradiate the sample with a Maxwellian neutron beam and directly extract the MACS value. Examples in [19, 20]

ii) Indirect measurements: Measure the point-wise cross section of the reaction under study and then fold it with a Maxwellian spectrum to extract the MACS, according to 1.4 and the reaction's astrophysical impact. Example in [21].

$$< \sigma >= \frac{< \sigma > v}{v_T} = \frac{2}{\sqrt{\pi}} \frac{1}{kT} \int_0^\infty \sigma(E) E exp-(\frac{E}{kT}) dE \tag{1.4}$$

with

- $\langle\sigma\rangle$ – MACS.
- $\langle\sigma v\rangle$ – Reaction rate per particle pair.
- v_T – Thermal velocity, representing the characteristic speed of particles at temperature T.
- k – Boltzmann constant (1.38×10^{-23} J/K).
- T – Temperature of the system in Kelvin.
- $\sigma(E)$ – Energy-dependent cross-section for the interaction.
- E – Energy of the interacting particles.

1.3 Motivation

The neutron time-of-flight (n_TOF) facility at CERN is already present at MACS measurements via time-of-flight (TOF) and the collaboration behind it is constantly proposing new developments and ideas [22]. Accordingly, a new experimental area was constructed in 2021 with the aim of being exploited for even more astrophysical studies [23]. Despite the growing body of research on neutron capture reactions using the TOF technique, limitations in the available sample mass can sometimes hinder its application. This issue particularly arises when dealing with unstable isotopes. In such cases, where only extremely small sample masses are available, or when considering extremely small reaction cross sections, integral measurements through the activation technique remain a viable option. This approach allows access to previously unexplored physics cases. The sensitivity and selectivity of the activation technique can play a vital role in achieving challenging measurements or even in benchmarking previous studies conducted using the TOF technique.

The purpose of this study is to investigate the possibility of extracting MACS values through integral measurements at n_TOF's newest experimental area. In order to achieve this, the 11-orders-of-magnitude-spanning n_TOF neutron energy distribution has to be modified so it resembles a Maxwell-Boltzmann distribution as closely as possible. This study is thus a feasibility study of one possible method of shaping the neutron energy distribution, which is the employment of suitable filters.

To validate the method, samples with neutron capture cross sections of different shapes already measured and well-known are irradiated together with a reference foil, again of a known cross section. The induced activity is

measured after the irradiation and the number of activated nuclei produced during the irradiation can be estimated. The ratio of the activated nuclei is directly proportional to the ratio of the cross sections of the sample and reference foil, with each cross section being in fact a "spectral averaged" cross section (SACS), meaning an average value of the cross section for this specific neutron spectrum. We can then compare the ratio of these SACS with that of the ideal MACS we would have, if the neutron spectrum was perfectly Maxwellian. This comparison alone can give us a hint as to whether we can measure SACS and extrapolate the values of the corresponding MACS. Furthermore, by comparing that ratio to Monte Carlo simulations, we can validate them, leading to a trustworthy determination of the neutron energy distribution shape itself, through these simulations.

This study is a qualitative control of this shaping method using filters and can quantify how far we are from the "ideal" case of a purely Maxwellian beam.

2 Methodology and physics cases

2.1 The activation technique

The principle of the activation technique is rather old, dating back to 1936 when Hevesy and Levi first implemented it to extract the amount of dysprosium in an yttrium sample [24]. Thanks to its extremely high sensitivity, high selectivity and its being a non-destructive experimental method, the activation technique is now a powerful tool in various scientific fields as well as industry.

This technique consists of two stages: The irradiation of the sample in beam, inducing nuclear reactions that produce various nuclei, and the subsequent measurement of the induced activity. It can be both qualitative, aiming for example to the identification of some unknown isotope through the unique properties of the radiation it emits, or quantitative, where the mass of an element, the particle flux or an unknown cross-section can be determined.

Whether the activation technique can be employed for the study of a particular physics case depends on the decay characteristics of the produced isotope. If the half-life is too short, the resulting activity is very low and a measurement is highly impractical. If, on the other hand, the half-life of the isotope is too long, the irradiation and measurement times need to be significantly increased to lead to adequate statistics. Furthermore, the radiation emitted during the isotope's decay should not present excessive counting difficulties. For example, if an isotope decays by emitting a gamma-ray with very low intensity, the counting rate is extremely low rendering the activation technique unsuitable for its study [25].

The number of nuclei of interest after irradiation is given by:

$$N_{act} = \sigma N_T \Phi f_B \tag{2.1}$$

and the formula to derive the cross-section of a reaction employing the activation technique is the following:

$$\sigma = \frac{counts * corrections}{\Phi \epsilon I N_T e^{-\lambda t_{wait}} \left(1 - e^{-\lambda t_{meas}}\right) f_B} \tag{2.2}$$

with

- *counts* the number of counts recorded in the experimental spectrum

- *corrections* the various correction factors we need to apply to our counts, such as self-attenuation, dead time, etc.
- Φ the incident particle flux as $particles/cm^2$
- ϵ the detection efficiency
- I the emitted radiation intensity
- N_T the number of nuclei in our sample (target nuclei)
- t_{wait} the elapsed time between the end of the irradiation and the beginning of the measurement ("waiting" or "cooling" time)
- t_{meas} the measurement time
- f_B a correction factor accounting for the nuclei that decayed during the irradiation period. Details about this correction factor can be found in 6.2

The activation technique formula is directly derived from the differential equation that describes the rate of nuclei formation during irradiation:

$$\frac{dN_{act}}{dt} = \sigma f(t)(N_T - N_{act}) - \lambda N_{act}$$

The step-by-step solution of this differential equation can be found in 6.1.

2.2 The physics cases

In order to test the effectiveness of the use of filters in shaping the neutron energy distribution of the NEAR Station into a quasi-Maxwellian one, suitable reactions with already known cross section had to be selected. For this purpose, four reactions were chosen: neutron capture on ^{140}Ce, ^{94}Zr, ^{197}Au and ^{76}Ge. Experimental cross section data for these reactions are already available coming from different measurements at different facilities. All of these cross sections have been measured at n_TOF as well, with some of the results already published [26–29]. Figure 8 shows the cross sections of four of the above reactions as given by TENDL-2019 [30].

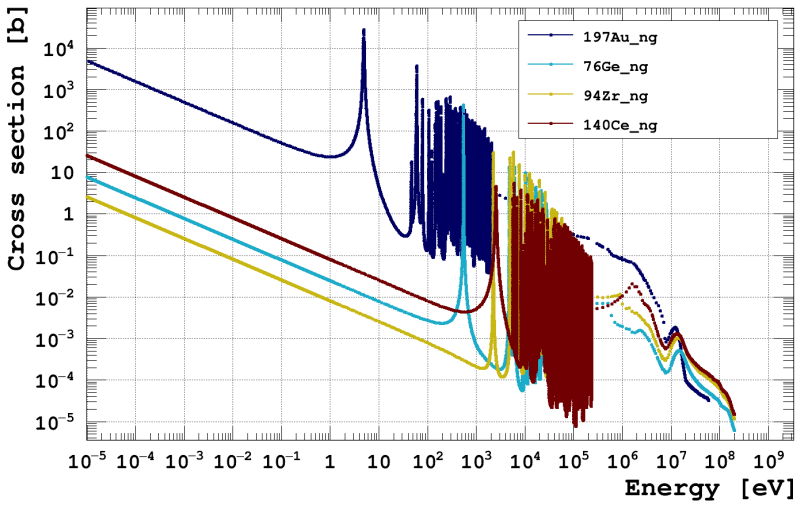

Figure 8: Neutron capture cross sections for four of the reactions used [30].

2.2.1 ^{76}Ge(n,γ)

Natural germanium consists of 5 stable isotopes, with ^{76}Ge being the heaviest one. After capturing a neutron, ^{76}Ge produces ^{77}Ge, an unstable nuclei with 11.3 hours of half-life which decays via β-decay to ^{77}As. The decay scheme can be seen in Fig. 9. The three most intense photopeaks of this decay have an energy of 215.5 keV, 265 keV and 416 keV. None of them can be contaminated by any natural background γ-ray of similar energy, however the (n,2n) reaction on ^{76}Ge produces ^{75}Ge, which decays by emitting, among others, a 264.5 keV γ-ray which can overlap with ^{77}Ge's 265 keV photopeak. ^{75}Ge has a half-life of $\sim$ 83 min.

2.2.2 ^{94}Zr(n,γ)

^{94}Zr is one of the five stable isotopes of zirconium. When capturing a neutron, it produces ^{95}Zr which decays to ^{95}Nb via β-decay, according to the scheme in fig. 10. From this decay, two γ-rays are emitted, with energies of 756.7 keV and 724.2 keV. ^{95}Zr can also be produced by the (n,2n) reaction on zirconium's heaviest isotope ^{96}Zr, thus a correction needs to be applied in the data analysis phase to account for the population of ^{95}Zr through this (n,2n) channel.

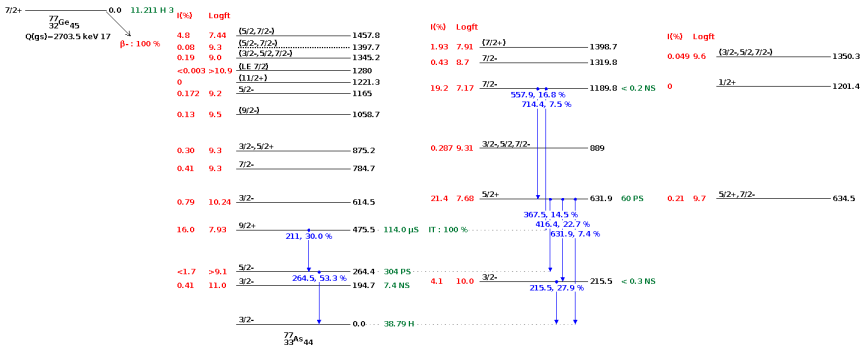

Figure 9: Decay scheme of ^{77}Ge [31].

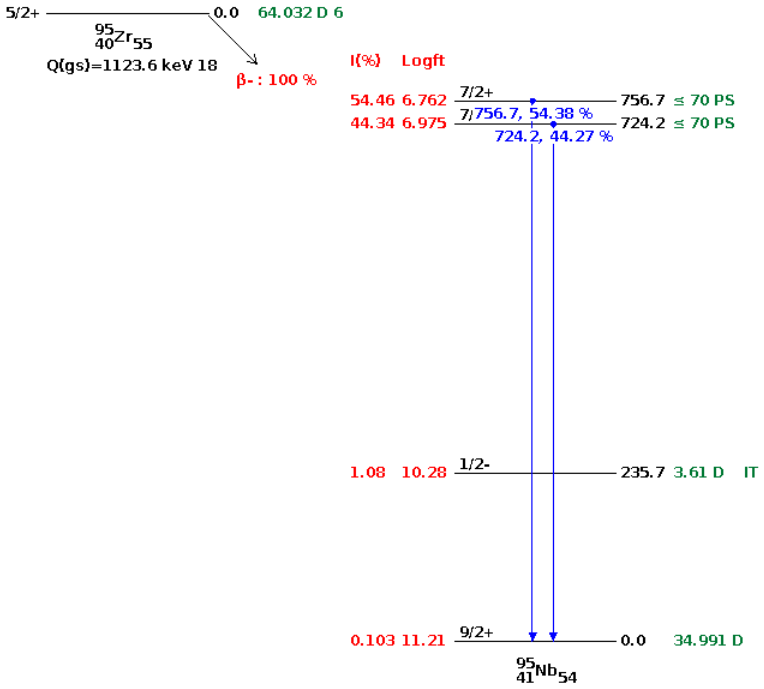

Figure 10: Decay scheme of ^{95}Zr [32].

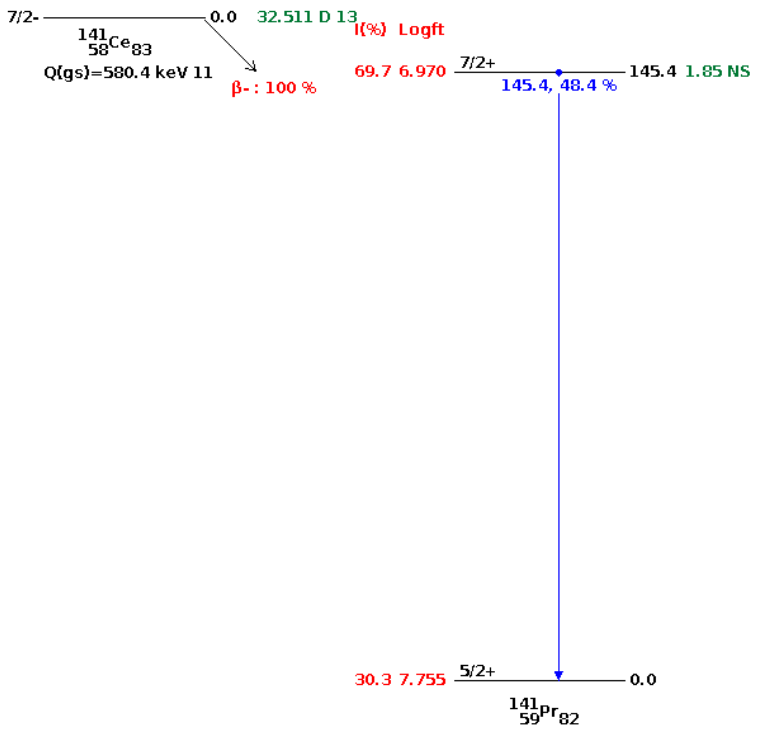

Figure 11: Decay scheme of ^{141}Ce [33].

2.2.3 ^{140}Ce(n,γ)

^{140}Ce is the most abundant stable isotope of cerium. When undergoing a neutron capture reaction, ^{141}Ce is produced and decays to ^{141}Pr via β-decay, according to the scheme in fig. 11. Following this decay, a γ-ray of 145 keV is emitted. ^{141}Ce can also be produced by the (n,2n) reaction on ^{142}Ce, thus a correction needs to be applied, similarly to the case of ^{95}Zr.

2.2.4 ^{197}Au(n,γ)

^{197}Au is the only stable isotope of gold. The ^{197}Au(n,γ) reaction produces ^{198}Au which, with a half-life of 2.69 days, decays into ^{198}Hg emitting a γ-ray of 412 keV.

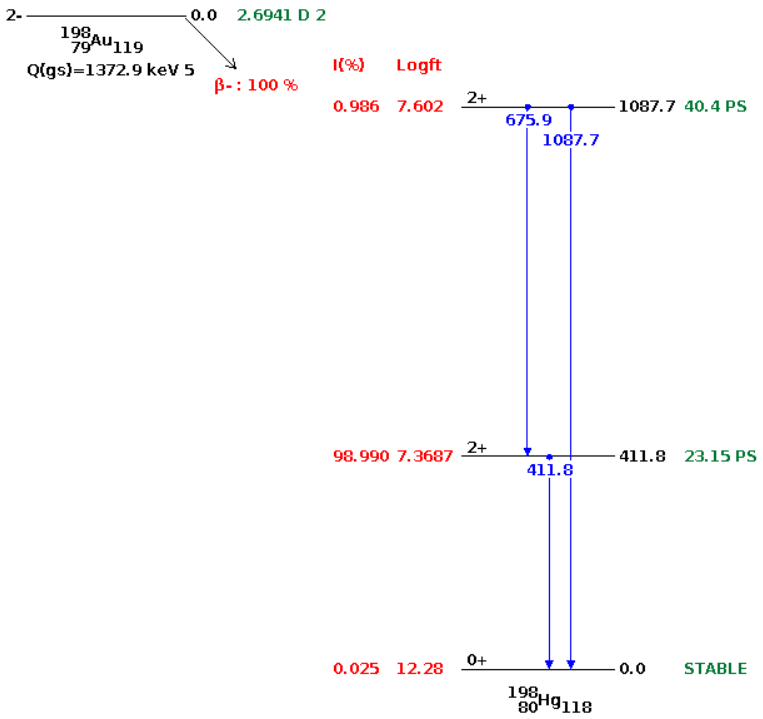

Figure 12: Decay scheme of ^{198}Au [34].

3 Experimental Set-up

The aim of this work is to explore the possibility of integral MACS measurements at the NEAR station of n_TOF. In this chapter the n_TOF facility as well as the NEAR station are described, together with the dedicated experimental setup used in this feasibility study.

3.1 The n_TOF facility

The n_TOF facility is CERN's neutrons spallation source. It was first envisioned in 1998 by C. Rubbia [35] and came into operation in 2001. Initially consisting of only the spallation target and one beam line [36], the facility underwent various upgrades leading the development of two more experimental areas [37, 38] in 2014 and 2021. More details on the characteristics of all the experimental areas as well as a description of the basis of the facility operation, the neutron production through spallation, are given in the next paragraph.

The aim of this facility is to study neutron induced reactions important for different fields of nuclear physics, starting from basic research and extending to, among others, nuclear astrophysics [39, 40], nuclear technology applications [41] and nuclear medicine [42]. It is operated by the n_TOF collaboration, which comprises $\sim$ 40 member institutes.

3.1.1 Neutron production

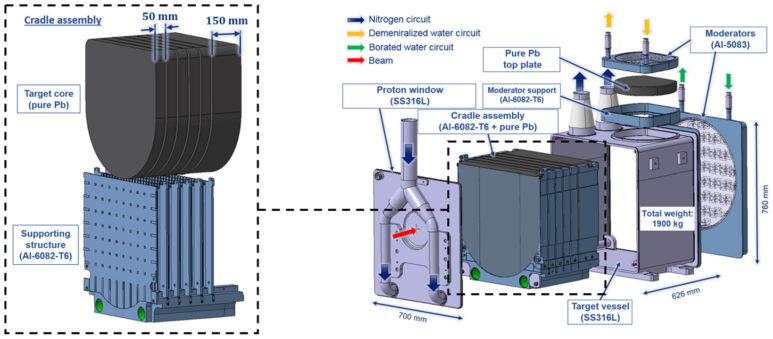

Figure 13: Schematic representation of the n_TOF target #3. [43].

Neutrons are one type of the many particles produced by spallation reactions when a 20 GeV/c proton beam delivered by CERN's PS accelerator impinges on the facility's lead spallation target. This proton beam is pulsed,

with the maximum repetition rate achievable being 0.8 Hz (or one bunch every 1.25 seconds), however the actual repetition rate of each experiment depends mainly on the beam demands of the CERN accelerator complex, as well as the maximum power the spallation target is able to sustain. The maximum repetition rate being relatively low grants the advantage of no possible overlapping of consecutive pulses, even for very low energy neutrons. Two types of proton pulses are delivered to the n_TOF target: "dedicated" ones, with an average intensity of 850×10^{10} protons, and "parasitic" ones of lower intensity, around 300×10^{10} protons.

The spallation target consists of 6 pure lead slices, all of them 60 cm in length and height with 5 of them having 5 cm thickness, while the last one having a thickness of 15 cm in order to keep the background as low as possible. The slices are supported by an aluminium-alloy structure which also contains channels that regulate the flow of nitrogen gas used for cooling [43]. A schematic representation of target #3 can be found in Fig. 13.

As neutrons produced through spallation have in general high energies, they need to be moderated if a broad energy spectrum is desired. The two experimental areas of n_TOF use two different moderating materials: demineralised water for EAR2 and borated water for EAR1. This difference in the moderating material is reflected in the shape of the neutron fluence of each area, with EAR2 featuring a very prominent thermal peak contrary to EAR1, for which this thermal peak is suppressed due to the capture of thermal neutrons by ^{10}B. The demineralised water also helps suppress the 2.2 MeV γ-ray produced by neutron capture in hydrogen.

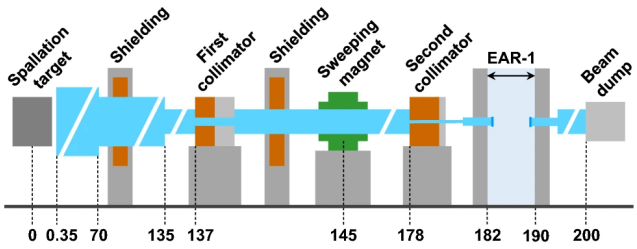

Figure 14: Schematic representation of the n_TOF 185 m beam line. Taken from [41].

3.1.2 The two time-of-flight beam lines

The neutrons produced after the spallation reactions emerge from the target and moderator assembly with various energies covering 11 orders of magnitude (from thermal to GeV). In order to extract energy dependent results, one needs to know the exact energy of every neutron. This can be achieved through the time-of-flight technique in the Experimental Areas 1 & 2 of the facility. This technique allows for the determination of a neutron's energy, based on the time it takes to travel a fixed flight path. The longer this flight path, the better the energy resolution.

EAR1 is located at the end of an approximately 185 m long beam line which forms a 10^o angle with the incident proton beam. This angle helps in decreasing the background caused by other particles produced during the spallation processes and which are highly directional. To further decrease background by preventing any charged particles from reaching the experimental area, a magnet is placed at a distance of approximately 145 m after the spallation target. Two collimators are also installed in the beam line, the first of which is located before the sweeping magnet, while the second one is located before the experimental hall and has two different aperture options, depending on each experiment's needs in neutron fluence and beam size [41]. A schematic representation of the beam line and its most important elements can be found in Fig. 14.

EAR2 is located directly above the spallation target, at the end of a 19 m vertical beam line. As in the case of EAR1, this beam line also consists of a sweeping magnet and two collimators, with the second one having two different options as to its inner diameter [44]. The layout of EAR2 can be seen in Fig. 15.

Even with all the shielding and background reducing elements of the beam lines, a component consisting of γ-rays as well as relativistic particles referred to as "γ-flash", always reaches the experimental areas and induces a large signal in most detectors. This component travels at almost the speed of light and the signal it induces can be used as the "starting point" for the time-of-flight of the neutrons.

EAR2, being at the end of a shorter beam line than EAR1, is characterised by lower energy resolution, however, it offers a higher signal-to-background ratio thanks to its higher instantaneous neutron fluence. This makes it suitable for challenging measurements of low mass or even radioactive samples. Each experimental area and/or the combination of the two can offer different advantages to different types of measurements. More details on the characteristics of the n_TOF experimental areas can be found in [41,

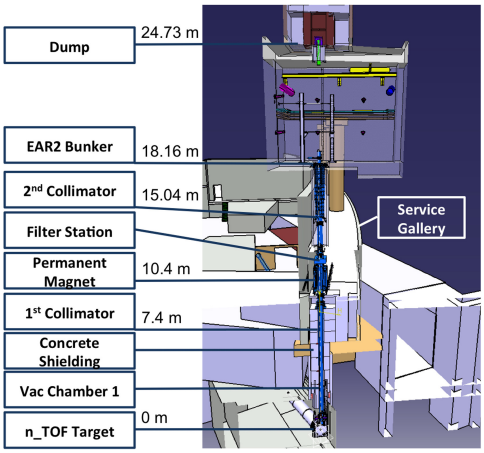

Figure 15: Schematic representation of the n_TOF 20 m beam line. Taken from [44].

44–47].

3.1.3 The NEAR Station

The idea of a new experimental area at n_TOF was formed during CERN's Long Shutdown phase of 2019-2021 (LS2)[38]. During LS2, the n_TOF target shielding was completely overhauled and modified in order to allow access to the target pit. The lead spallation target was removed and replaced with a new generation one, as seen in Fig. 16, better optimised to enhance the beam characteristics of the facility's two beam lines. Together with these modifications, a new experimental station was designed and developed in close proximity to the target, profiting from high instantaneous flux. This new station, the "NEAR" Station, will be discussed in detail in the next paragraphs.

3.1.3.1 Technical characteristics

The NEAR Station owes its name to its proximity to the spallation target. It comprises two "areas", the NEAR "Irradiation" Station (i-NEAR) and the NEAR "activation" station (a-NEAR), with the first being directly next to the spallation target and dedicated to the study of radiation effects to materials, and the second one being located just outside the target bunker shielding. This shielding consists of three layers, an innermost layer of 400 mm stainless steel, a second layer of 800 mm concrete and an outer layer

(a) Production (b) Installation

Figure 16: The new spallation target. Photos: CERN

of 200 mm thick marble. It is mounted on steel rails and can be manually opened in order to allow access to i-NEAR [48].

The neutron beam reaches a-NEAR through a hole in the previously described shielding. The hole houses a movable collimating system, consisting of a 50 cm stainless steel part and a second part of borated polyethylene disks[48]. In a-NEAR, challenging activation measurements can be performed, thanks to the station's high flux that allows the study of low-mass or highly radioactive samples. a-NEAR is equipped with an Aluminium rail bolted on the marble shielding and aligned with the collimator, acting as a support for all the experimental setups measured at the activation station. The outermost layer of the target bunker shielding, along with the setup support, can be seen in Fig. 17.

The neutron beam then continues to the wall opposite the collimator exit, approximately 2.5 m away from the measuring point of a-NEAR. Additional irradiations, for example of electronic devices, can take place on that spot.

3.1.3.2 The FLUKA simulations

The experimental conditions of the NEAR Station were extensively investigated via simulations performed with the FLUKA code [49, 50] by the CERN-FLUKA group. The results of these simulations can be summarised in the following graphs. An important conclusion is that the position at 20 cm from the exit of the collimator (at the end of the marble shielding) represents the best compromise between beam dimensions and neutron background. It has thus been chosen as the irradiation position for most samples and campaigns. Another key conclusion is that the amount of hadrons other than neutrons exiting the collimator amounts to only 0.3% of the total num-

Figure 17: An overview of a-NEAR. The outermost layer of the target bunker shielding, a 200mm thick layer of marble and the Aluminium supporting rail can be seen.

ber of particles exiting.

3.1.3.3 The Multi-foil activation characterisation

To validate the FLUKA simulations of the NEAR Station, a set of experimental flux measurements was designed, one of which was based on the multi-foil activation method. In this method, many foils of elements with well-known cross sections are irradiated and their induced activity is measured, as per the activation technique [23, 51, 52]. Afterwards, each reaction rate is calculated and used as an input to "unfold" the incident neutron energy distribution[53, 54].

The "MAM1" measurement was one of the three separate measurements of this multi-foil activation campaign, and it employed the 14 samples presented in Table 2. The reactions studied were a combination of capture reactions, sensitive in general to low energy neutrons, and (n,cp) as well as (n,xn) reactions, which are threshold reactions, thus sensitive only to neutrons with energies higher than their respective threshold energy. The foils were placed in two identical holders, which were placed along the beams path one behind the other, approximately 20cm away from the collimator exit, as seen in Fig. 20

After a three-week irradiation period, the foils were removed from the beam's path and their induced activity was measured with a High Purity germanium (HPGe) detector of 25% relative efficiency. The HPGe had been previously [55] characterised with the Geant4 [56–58] simulation toolkit, with the resulting model being used for the extraction of the measurement

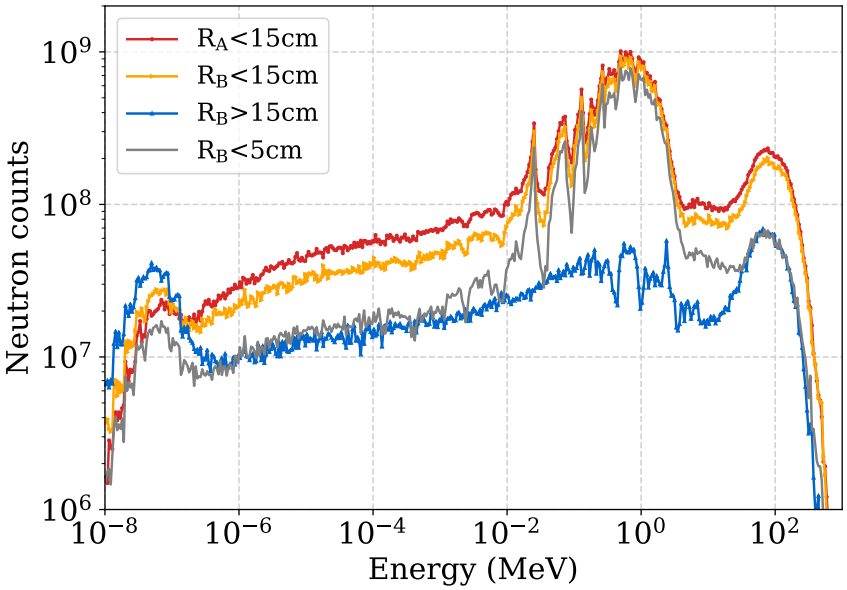

Figure 18: Resulting NEAR neutron spectra from FLUKA simulations for different scoring plane radius. Position A stands for neutrons scored exactly at the exit of the collimator, while the position at 20 cm from it is denoted position B. Courtesy: M. Cecchetto.

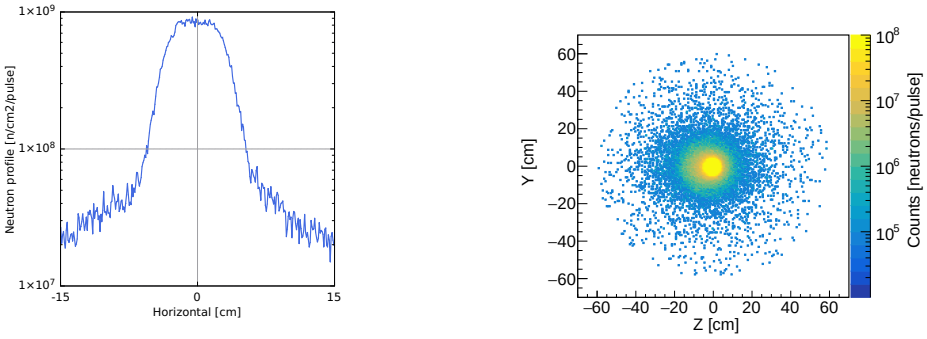

(a) Profile of the beam (1D)

(b) Profile of the beam (2D)

Figure 19: Profile of the neutron beam at position B (20 cm from the collimator exit). Courtesy: M. Cecchetto.

Sample ID	Radius [cm]	Thickness [mm]	Mass [g]
Cd	0.65	0.1	1.0714
Sc	0.15	0.03	0.0073
Au-1	0.15	0.05	0.0709
Au-2	0.15	0.05	0.0712
Au-6	0.65	0.0025	0.0550
Au-3	0.15	0.01	0.0142
Au-4	0.15	0.01	0.0149
Au-backup	0.15	0.01	0.0148
W	0.65	0.05	1.2349
In	0.65	0.05	0.4675
Ni	0.65	0.05	0.5624
Al	0.65	0.05	0.1694
Co	0.15	0.05	0.0348
Bi	0.65	0.1	1.1070

Table 2: The samples used for the MAM1 flux extraction

(a) Side view (b) Front view

Figure 20: The holder-foils assembly for MAM1 placed on the support rail at a distance of 20cm from the collimator exit

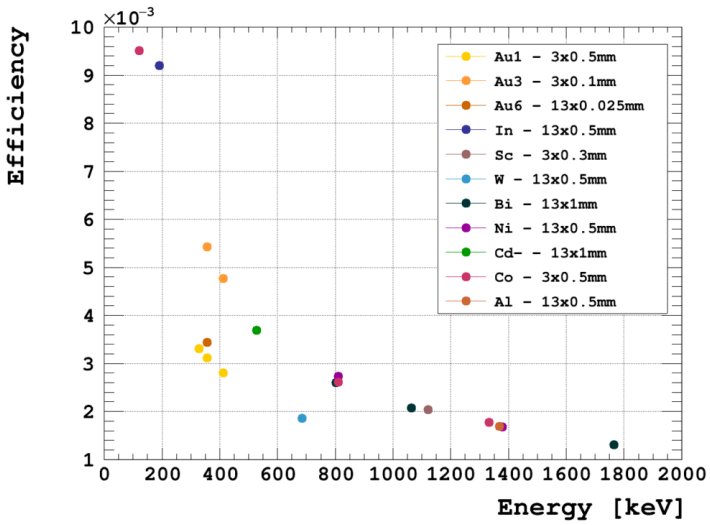

Figure 21: The detection efficiency for each foil, as extracted through Monte Carlo simulations using the Geant4 simulation toolkit

efficiency taking into account each sample's geometry as well as each isotope's decay scheme. The extracted efficiency can be seen in Fig. 21.

The reaction rate for each reaction of interest was then calculated from the activity data and used as an input for the flux "unfolding", along with the reactions cross sections. The resulting flux and its comparison with the NEAR FLUKA simulations is presented in Fig. 22. As can be seen, simulations and experiment agree within a few error bars in the thermal and epithermal energy regions, while for higher energies agreement is achieved within 20-30%.

3.2 The irradiation set-up

The irradiation set-up of this work consisted of the B_4C filter, the sample and reference sample combination as well as two aluminium rings for the sample's encapsulation and alignment. The whole assembly was held together with the help of an aluminium support, specially designed to keep it tight and in vertical position but with the minimal amount of material in beam. The details of the set-up are described in the following paragraphs. An example of one configuration placed in its irradiation position is shown in Figure 23.

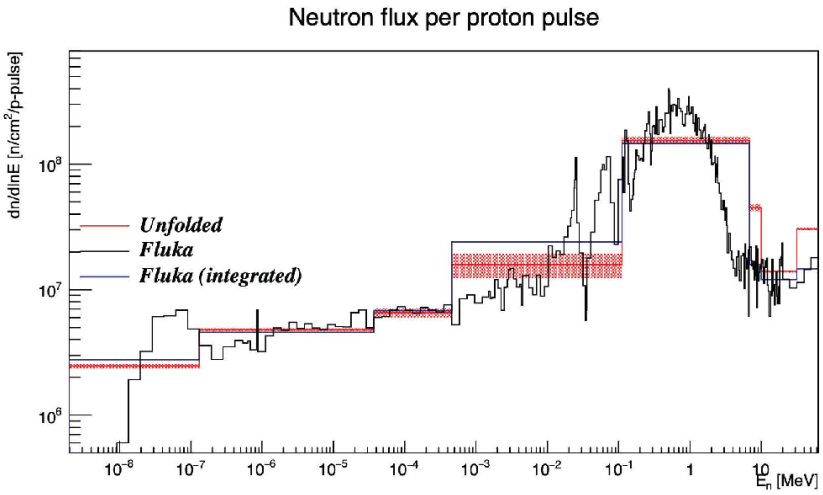

Figure 22: In red: The neutron flux of a-NEAR, as resulted from the MAM1 measurement. In black: The FLUKA simulation results. Courtesy: M. Mastromarco

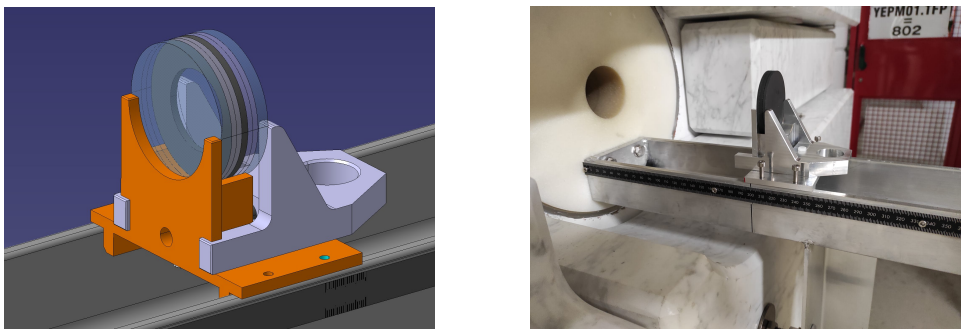

(a) (b)

Figure 23: (a) A schematic representation of the irradiation setup (b) Example of sample-filter assembly in its irradiation position

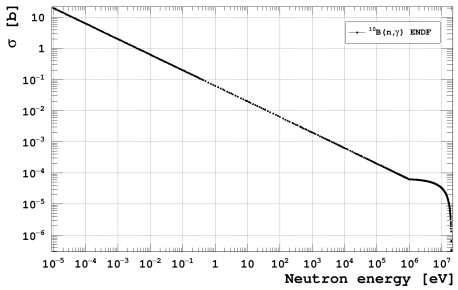

(a)

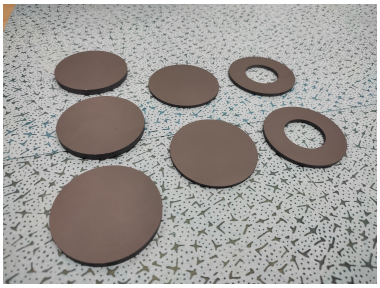

(b)

Figure 24: (a) The neutron capture cross-section of ^{10}B as a function of the incident neutron energy. Data from ENDF/B-VIII.0 [59] (b) B_4C filter details

Shape	Diameter [mm]	Thickness [mm]	Mass [g]	Quantity
Ring	60	3	15	2
Disk	60	2.5	16	2
Disk	60	5	33	3

Table 3: Characteristics of the B_4C filtering pieces.

3.2.1 The filters

In order to shape the incident neutrons' energy distribution, filters made of B_4C enriched in ^{10}B were employed. ^{10}B has a very high neutron capture cross-section, so it can be used to absorb the thermal and epithermal neutrons of the spectrum. The ^{10}B(n, γ) cross-section as a function of the incident neutron energy can be seen in Fig. 24 (a).

The filtering set-up consisted of 7 pieces of B_4C of different shape and dimensions. Disks of varying thickness were used in front of and to the back of the sample, while a central ring-shaped piece was also used, aiming to completely surround the sample with the filtering material. The B_4C disks can be seen in Fig. 24 on the right and their characteristics are summarised in Table 3.

To achieve different Maxwellian distributions matching different temperatures, the pieces mentioned above were combined to form filters of various thicknesses. Each time the sample was placed in the hole of the ring-shaped piece together with a gold foil used as reference and the different pieces were

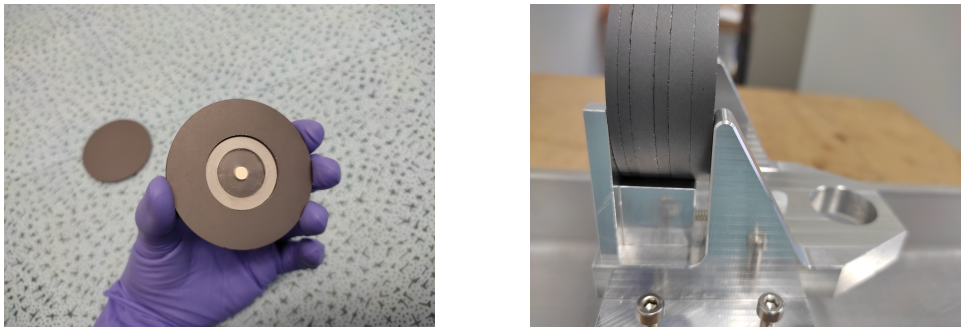

(a) A sample placed in the ring (b) Example of 10mm thick filter

Figure 25: An example of a sample-filter assembly

Sample ID	Material	Mass [g]	Thickness [mm]	Form
Ce1	CeO_2	0.20248	2.2	Pellet
Ce2	CeO_2	0.20247	2.2	Pellet
Ce3	CeO_2	0.2088	2.2	Pellet
Ge	$GeO_2 + cellulose$	0.118	2.1	Pellet
AuS1	Au	0.00855	0.025	Metallic foil
AuS2	Au	0.00870	0.025	Metallic foil
AuS3	Au	0.009425	0.025	Metallic foil
Zr1	Zr	0.187	-	Lumps
Zr2	Zr	0.093	-	Lumps

Table 4: Characteristics of the samples used in this study. All of them had a diameter of 5mm.

used to "sandwich" the sample between them. An example of the sample placement and the final assembly can be seen in Fig. 25.

3.2.2 The samples

As previously discussed in 2.2, four reactions were chosen for this feasibility study: neutron capture on ^{140}Ce, ^{94}Zr, ^{197}Au, and ^{76}Ge. In order to perform the necessary measurements with the different filter thicknesses, various samples had to be produced. Table 4 summarises the characteristics of each sample, such as its ID, its mass and physical form.

In the case of Ce, the isotope of interest ^{140}Ce is naturally the most abundant one, so the sample was created pressing natural CeO_2 powder.

Isotope	Abundance/Enrichment (%)
^{140}Ce	88.45
^{142}Ce	11.114
^{74}Ge	11.33
^{76}Ge	88.46
^{94}Zr	91.2
^{96}Zr	1

Table 5: Isotopic composition of Cerium, Germanium and Zirconium samples (only isotopes with abundance $\geq 1\%$ are shown).

(a) Ce pellet centered with respect to the Al ring

(b) Three Ce pellets being encapsulated in a thin Mylar foil

Figure 26: Example of pellet sample preparation

Au is a monoisotopic element so the samples were cut from natural Au metallic foils. In the case of ^{76}Ge and ^{94}Zr, enriched material was needed. The Ge sample was created by pressing a mixture of $^{76}GeO_2$ and cellulose, in order to increase the mechanical stability of the sample, while for the Zr measurement, metallic lumps enriched in ^{94}Zr were used. The isotopic composition of the enriched samples can be found in table 5 (most abundant isotopes).

In order for the samples to be aligned with respect to the collimator exit as well as vertically fixed within the central B_4C filter ring, aluminium ring supports were employed. Furthermore, for radiation protection reasons, the samples were encapsulated in mylar, kapton or teflon foils. Figure 26 shows an example of a pellet sample centering on its aluminium supporting ring and following encapsulation between two mylar foils.

Element	Dimension [mm]
Entrance window diameter	68
Window to crystal distance	7.5
Crystal length	66.5
Crystal radius	68.5

Table 6: The dimensions of the HPGe detector crystal as obtained from the specification sheet provided by the manufacturer.

3.3 The activity measurement set-up

After the irradiation of each sample, the induced activity needs to be measured. The type of detector chosen for this measurement in this work was High Purity Germanium (HPGe), in order to profit from the excellent energy resolution these detectors offer.

3.3.1 The HPGe

The HPGe used for activation measurements at the n_TOF facility is a CANBERRA GR5522. It is an n-type HPGe and has a relative efficiency of 63%. Its entrance window is made of thin carbon, allowing for recording even very low energy photons. It is cooled by means of the CANBERRA CP-5 electrically refrigerated cryostat. Moreover, its charge sensitive preamplifier is equipped with a fast-switch circuit which grounds excessive charge for a time given by the user [60]. In this way the detector can also be used for time-of-flight measurements in the other two n_TOF experimental areas without suffering from the large prompt signal, the γ-flash, observed there. The presence of this circuit does not affect at all the spectroscopic characteristics of the detector.

In order to improve background conditions, the detector is located in a dedicated underground area, the "GEAR" Station (Gamma spectroscopy Experimental ARea) and is placed inside a CANBERRA 747 lead shield of 10 cm thickness, lined with 1.6 mm of copper [61]. A photograph of the shielding together with a background spectrum can be found in Figure 27. The characteristic dimensions of the detector as found in the specifications sheet are summarised in Table 6. The readout electronic chain consists of a Canberra 2026 Spectroscopy amplifier and the AmpTek model 8000D Multi-Channel Analyser (MCA) together with its digital pulse processing (DPP) software.

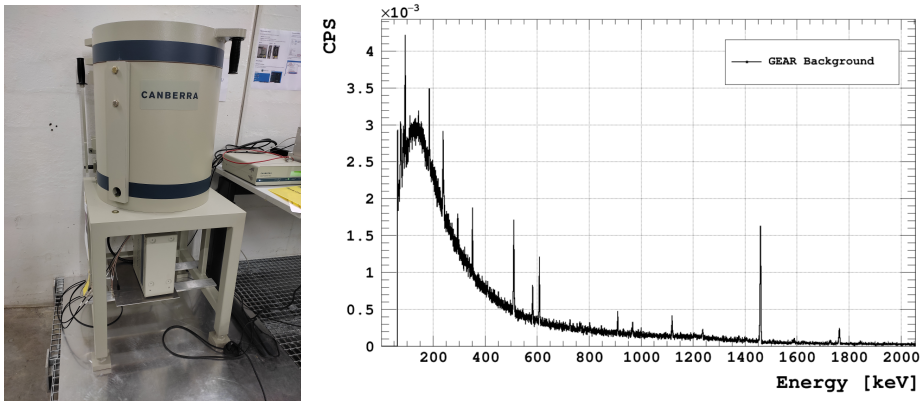

(a) HPGe detector (b) Background spectrum

Figure 27: Left: The HPGe detector placed inside its lead shielding. Right: Background spectrum at the GEAR Station

3.3.2 HPGe efficiency calibration

When performing an activity measurement, one of the variables needed is the detection efficiency, as shown in 2.1 and proven in 6.1. This depends on the detector intrinsic efficiency as well as the geometry of the measurement. A way to accurately estimate the detection efficiency is to experimentally characterise the detector using point calibration sources and to model it with a simulation toolkit. This model will subsequently be used to extract the detection efficiency, after the measurement realistic geometry has been implemented. For this work, the HPGe detector was characterised with the use of different calibration sources covering a wide energy range and then modelled in Geant4. The list of sources used as well as the photopeaks of interest for each one are summarised in Table 7. A plot of the experimental efficiency points can be found in 28.

For modelling the HPGe detector in Geant4, all its characteristic dimensions (crystal radius and length, distance between the crystal and the detector window, etc) were chosen according to the manufacturing company's specification sheet. However, as many previous studies and measurements have suggested (e.g. [62, 63]), there tend to be important discrepancies between the simulated values according to the manufacturer's specifications and the experimental values based on calibration sources. This discrepancy is particularly visible in low energy γ-rays, as it's affected by the dead layer thickness, which is not only difficult to measure but known to deteriorate

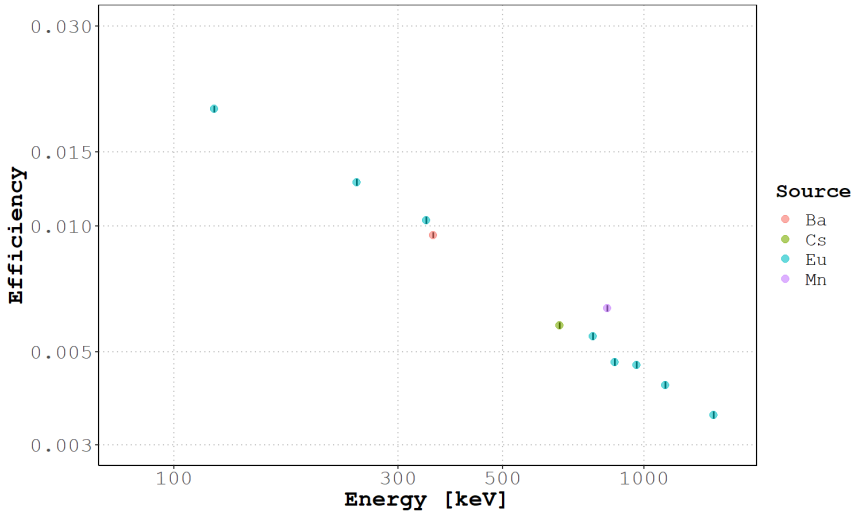

Figure 28: Experimental efficiency of HPGe detector. Points are colour-coded according to the calibration source that provided this γ-line.

Source ID	**Isotope**	**γ-ray energy [keV]**	**γ-ray intensity [%]**
RP#3693	^{152}Eu	121.8, 244.7, 344.e, 778.9	28.9, 7.5, 26.6, 12.9
RP#4845	^{152}Eu	867.4, 964.1, 1112.1, 1408	4.2, 14.5, 13.7, 20.9
RP#4023	^{137}Cs	661.66	85.1
RP#5069	^{54}Mn	834.85	99.98
RP#12502	^{133}Ba	356	62.1

Table 7: Radioactive sources used for the HPGe characterisation

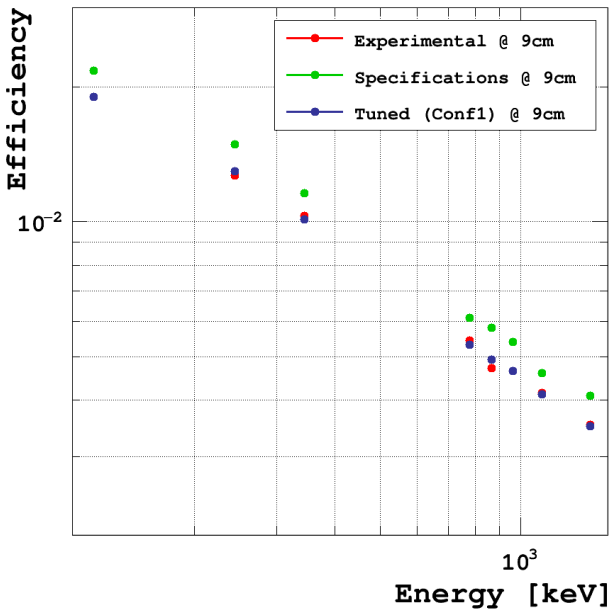

Figure 29: In red: Experimental efficiency of HPGe detector with a sample-to-detector distance of 9 cm. In green: Simulated efficiency according to the manufacturer's specifications. In blue: Simulated efficiency after tuning the detector's characteristic dimensions.

with time and use of the detector [64]. Fortunately, there exist two solutions for this problem. The first is to determine the true dimensions, for example via performing X-ray scans to the detector. This approach is accurate and of course difficult and costly. A second approach exists, and this is to manually fine tune all the values until the simulation accurately reproduces the experimental results [65, 66].

In this study, even though the HPGe detector was new, we also observed these expected discrepancies, as illustrated in Fig. 29. In order to resolve them, we decided to follow the second approach. The characteristic dimensions of the HPGe detector were manually altered until the resulting efficiency values were in satisfactory agreement with the experimental ones. The geometry used for the HPGe was purely cylindrical, with no rounding edges, the implementation of which is complex and not expected to significantly affect the efficiency at the gamma rays of interest for this work [67].

The code used for the geometry construction in our simulations can be found in the Appendices.

A graph of the detector efficiency as a function of γ-ray energy after this tuning process can be seen in Figure 30.

After matching the experimental with the simulated efficiency values for the calibration sources, the Geant4 model was used in order to extract the detection efficiency of the measurement. The geometry of the sample is introduced in the model, and the simulation primaries comprise the isotope of interest which then decays, producing all the γ-rays of interest. It has to be noted that, in this way of efficiency calculation, more correction factors are taken into account, such as any attenuation of γ-rays within the sample itself or any coincidence or random summing effects.

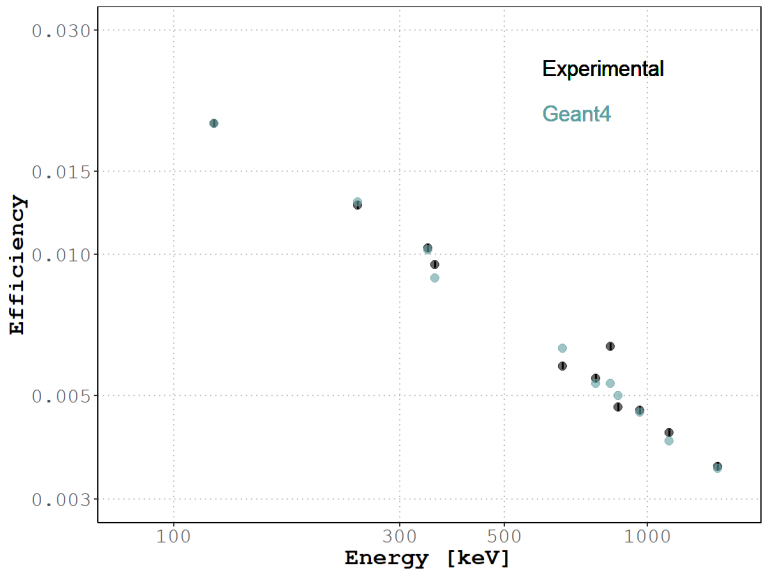

(a) Detection efficiency

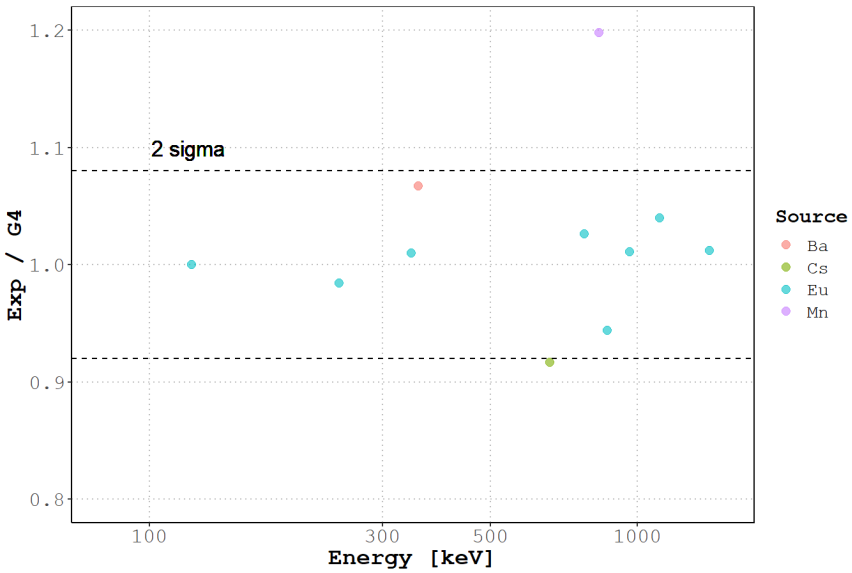

(b) Efficiency ratios

Figure 30: Top: Experimental and simulated efficiency. Bottom: Ratio between experimental and simulated efficiency

4 Data Analysis

4.1 Neutron flux simulations

In this study, the aim is to investigate the feasibility of MACS measurements of astrophysical interest by using B_4C filter to shape the neutron energy distribution into a Maxwellian one, centered around important temperatures of stellar evolution stages. In order to do this, we need to find a correspondence between filter thickness and temperature.

As discussed in chapter 3, extensive FLUKA simulations of the experimental conditions at NEAR have been performed, among which, various simulations of the neutron flux at different points. We can use their results as an input to a second simulation, one that propagates the NEAR neutrons through our experimental setup of filters and samples and yields as an output the filtered energy distribution. We can then fit the simulated distribution with a Maxwellian distribution and extract the corresponding temperature.

This second simulation was performed using the Geant4 simulation toolkit [56–58] and the results for the 4 filter thicknesses studied in this work can be found in Fig. 31. It should be noted that the results of the fit are very sensitive to the initial "guess" of the parameters. The results given in the figure use the energy of the bin with the maximum content as an initial "guess" for temperature and $2/\sqrt{\pi}kT$ as the initial guess for the normalisation.

4.2 The experimental spectra

After the irradiation of the samples, their induced activity was measured and the resulting γ-ray spectra were recorded. From those spectra, the number of counts in each photopeak of interest was extracted in order to be used in the calculation of the number of activated nuclei produced. The code used to analyse the spectra can be found in 6.3. An example of a γ-ray spectrum together with a background measurement (meaning a spectrum acquired without a sample on the detector) can be seen in Fig. 32.

4.3 Corrections

Before using the extracted number of counts in each photopeak of interest in the activation technique equations, several other factors have to be calculated. One of them is the detection efficiency at the exact geometry of the measurement, while the others are correction factors needed to account for the decay of some nuclei of interest during the irradiation time as well

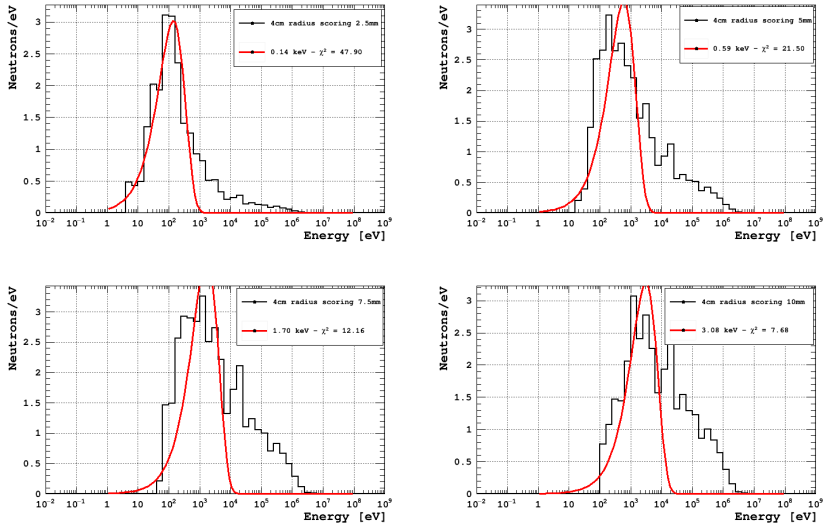

Figure 31: In black: Simulated energy distribution of NEAR neutrons. In red: Maxwellian fit. The four subplots represent the four different filter thicknesses.

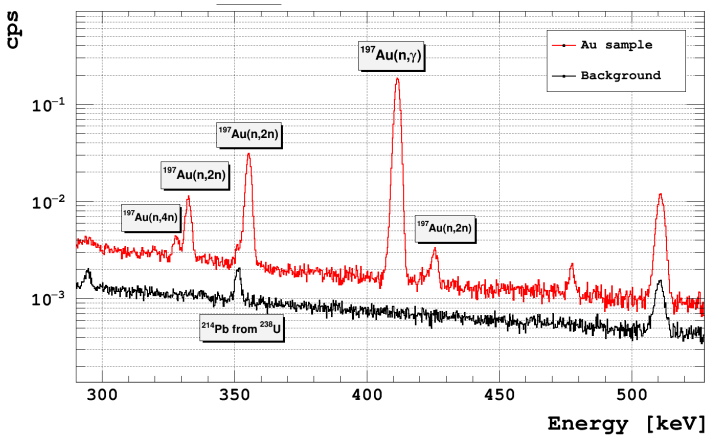

Figure 32: An example of a γ-ray spectrum recorded after the irradiation of gold sample AuS1. In red: the sample spectrum. In black: Background spectrum. Peaks of interest for our study are labelled.

for other competing reaction channels, meaning different reactions that also produce the nucleus under study.

4.3.1 Efficiency calculations

As described in 3.3, the detection efficiency of each experimental setup was extracted through extensive Monte Carlo simulations performed with the Geant4 toolkit, where all the details of the sample and detection geometry were carefully implemented. In this way, many needed correction factors, such as attenuation of the measured radiation inside the sample itself, summing effects, correction for hardware cuts applied, etc, are automatically taken into account.

For the efficiency simulation, the actual elemental composition of all samples was used and the density of the pressed powder samples was calculated according to their dimensions, as an "effective" density after pressing. Furthermore, the actual dimensions of the samples were used in all cases except for the ^{94}Zr sample. This sample consisted of metallic lumps of different shapes and sizes that could not be measured and modelled precisely, so it was approximated as a disk and a sensitivity study was carried out changing its dimensions and position. During the activity measurements, all samples were placed at 9 cm from the detector window, so this distance was also used in the simulations.

The uncertainty of the efficiency values was estimated to be 3%: The uncertainty in the activity of the calibration sources used ranged between 1.7% and 5% as measured by the service that provided them, while during the characterisation process, the values were tuned so that the deviation between the simulated and experimental results remained within a 3%. Furthermore, for the positioning of the samples and sources, a custom-made system of spacers was developed, allowing for excellent reproducibility and accurate knowledge of the sample-to-detector distance. A picture of these spacers together with one of a sample being placed on top of the detector window can be found in Fig. 33.

The efficiency results for the photopeaks of interest for this work are summarised in Table 8. The distance between the sample and detector was 9 cm. For comparison, the efficiency values taken from a linear fit of the calibration sources data, representing the efficiency without any correction for the sample's extended geometry, attenuation of γ-rays within the sample and summing effects, are given in the same table.

(a) Spacers to achieve different sample-to-detector distances

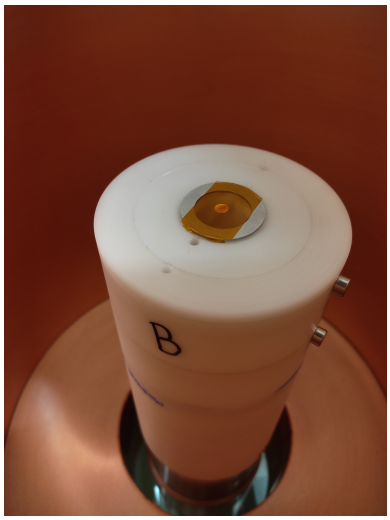

(b) Gold sample positioned 6 cm above the detector window

Figure 33: Left: An assembly of spacers used to fix the sample-to-detector distance. Right: A sample beeing measured at 6 cm from the detector window

Energy [keV]	**Reaction**	**Efficiency Fit**	**Efficiency Geant4**
145	^{140}Ce(n,γ)^{141}Ce	0.0179	0.0128
264	^{76}Ge(n,γ)^{77}Ge	0.0115	0.0117
412	^{197}Au(n,γ)^{198}Au	0.0083	0.0089
416	^{76}Ge(n,γ)^{77}Ge	0.0082	0.0084
724	^{94}Zr(n,γ)^{95}Zr	0.0055	0.0055
757	^{94}Zr(n,γ)^{95}Zr	0.0053	0.0053

Table 8: Detection efficiency at energies of interest. "Efficiency Fit" denotes the efficiency calculated by a fitting and interpolation of calibration sources data while "Efficiency Geant4" denotes the efficiency extracted from a full simulation, thus taking into account corrections such as the sample extended geometry, γ-ray self-attenuation in the sample and summing effects.

Sample ID	B_4C thickness [mm]	f_B
Ce1	5	0.906
Ce2	10	0.865
Ce3	15	0.915
Ce1	20	0.934
AuS1	5	0.455
AuS2	10	0.489
AuS3	15	0.482
AuS1	20	0.258
Ge	5	0.098
Ge	10	0.102
Ge	15	0.130
Ge	20	0.143
Zr1	5	0.930
Zr1	10	0.966
Zr2	15	0.968
Zr2	20	0.938
Y1	5	0.481
Y2	10	0.484
Y3	15	0.470
Y1	20	0.483

Table 9: f_B correction factor for all irradiations

4.3.2 Decay during irradiation time

As described in 2.1, during the irradiation time, some nuclei of interest are produced yet also decay. Those nuclei cannot be recorded in the subsequent activity measurement and they have to be accounted for through a correction factor, f_B. Details on the calculation of this correction factor are given in 6.2. The f_B correction factor for all the irradiations of this work is provided in Table 9.

4.3.3 Competing $(n, 2n)$ channels

In the case of cerium and zirconium, the nucleus of interest can be produced not only by the reaction under study, neutron capture, but also by (n,2n) reactions on heavier stable isotopes present in the sample. This only applies to cerium and zirconium, as the rest of the samples in this study are either

mono-isotopic or the heaviest stable isotope of that element. The contribution of these (n,2n) reactions in the production of the nucleus of interest has then to be estimated and subtracted.

In general, $N_{act} = \sigma N_T \Phi f_B$. Each channel has a different N_T since the target nucleus is a different isotope. Note that f_B depends on the λ of the product nucleus, which is the same for each reaction.

In the experiment, we measure $N_{act_{TOT}} = N_{act_{ng}} + N_{act_{n2n}}$ accounting to contributions from both channels. To find out how many originate from the capture that we're interested in, we need to subtract the contribution of the (n,2n) channel. We can do that by multiplying with a correction:

$$\frac{N_{act_{ng}}}{N_{act_{TOT}}} \tag{4.1}$$

And according to the above, this correction will be equal to:

$$\frac{N_{act_{ng}}}{N_{act_{TOT}}} = \frac{\sigma_{ng} N_{T_{ng}} \Phi f_{B_{ng}}}{\sigma_{ng} N_{T_{ng}} \Phi f_{B_{ng}} + \sigma_{n2n} N_{T_{n2n}} \Phi f_{B_{n2n}}} \tag{4.2}$$

or

$$\frac{N_{act_{ng}}}{N_{act_{TOT}}} = \frac{\sigma_{ng} N_{T_{ng}}}{\sigma_{ng} N_{T_{ng}} + \sigma_{n2n} N_{T_{n2n}}} \tag{4.3}$$

So, in order to calculate the correction we are interested in, we need the cross section of each reaction, for the neutron spectrum we have. Different evaluation libraries however, provide different values for the cross section, as can be seen in 34. Furthermore, the available data for most (n,2n) reactions are available only up to a specific energy and experimental data are scarce. Thus, the different possibilities for the 'extension' of this range need to be taken into account, as an additional 'uncertainty' in the resulting spectral-averaged cross section. An example, albeit an exaggerated one, of these different extension possibilities can be seen in 35.

The way the contaminating channel contribution subtraction is calculated in this study is the following:

- Point-wise (n,γ) cross section data from different evaluations are binned in a histogram with a binning so thin so as to be equivalent to the original graph.
- The (n,γ) cross section histograms are then re-binned to a thicker binning, matching the binning of our neutron spectra binning, as resulting from simulations. In this procedure, the integral of each bin is taken

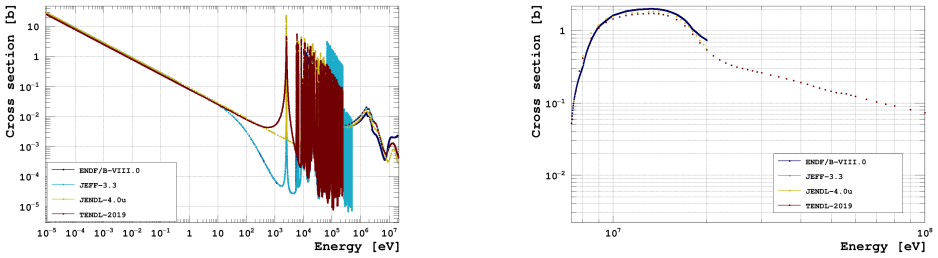

(a) 140Ce(n,g) (b) 142Ce(n,2n)

Figure 34: Example of cross section data from different evaluations

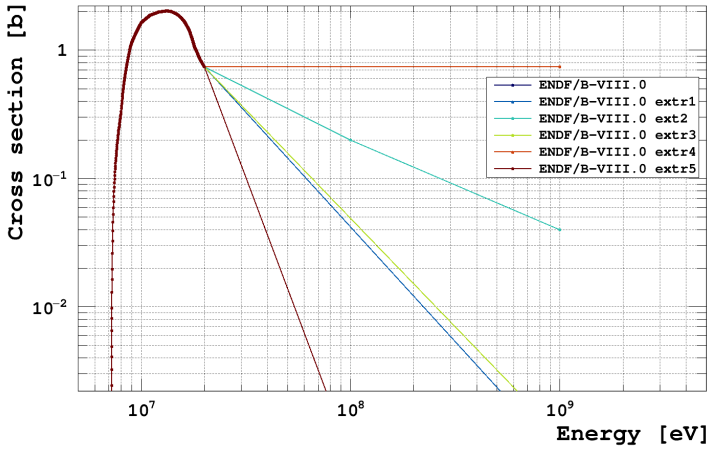

Figure 35: An example of different extrapolation possibilities for the (n,2n) reaction cross section on Ce-142.

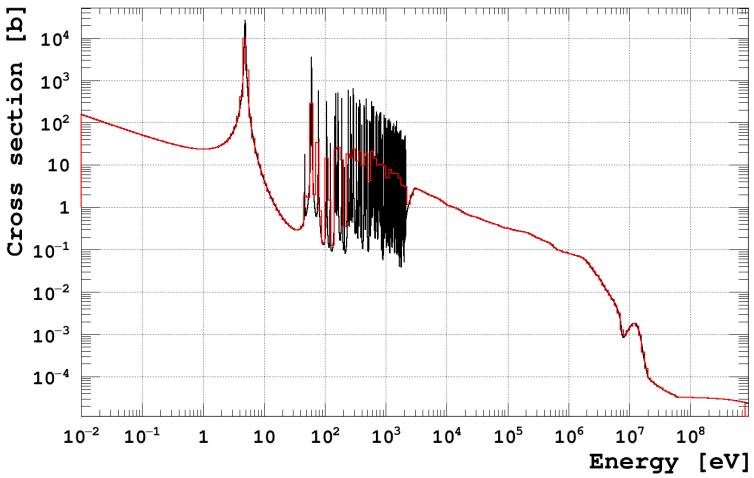

Figure 36: An example of a rebinned cross section. In black: The pointwise data as a graph. In red: The same cross section data represented as a histogram

into account, so as to conserve the correct information. An example of this process can be found in 36.

- The spectral-averaged cross section of the (n,γ) reaction is calculated by folding the two histograms (cross section and neutron fluence).
- A mean SACS as well as a spread are calculated for the different evaluation datasets.
- For the (n,2n) reaction cross sections, the above procedure is repeated with the addition of a step which calculates the SACS for some extreme extrapolation scenarios. Thus in this case, the final mean SACS and spread account both for the different evaluated data as well as the different behaviour of the cross section after the evaluation end point.

4.4 Spectral Averaged Cross Section ratios

Before continuing to the value of interest of this study, let's summarise the experimental procedure and analysis up to now. A sample and a reference gold foil were placed back to back and sandwiched between two B_4C disks. The configuration was then irradiated. After the end of the irradiation, both sample and reference foil were transported to the HPGe detector and

Sample	B_4C thickness [mm]	Correction factor	Spread (%)
Ce	5	0.56	6.2
Ce	10	0.54	5.9
Ce	15	0.53	6.4
Ce	20	0.51	6.9
Zr	5	0.71	6.4
Zr	10	0.70	7.1
Zr	15	0.68	7.9
Zr	20	0.67	8.7

Table 10: (n,2n) contribution subtraction correction factor for all cases affected

their induced activity was measured. The counts of the photopeaks were extracted and the number of activated nuclei, the nuclei produced from the neutron capture reaction of interest, were obtained, after correcting for their decay during both the irradiation time and the waiting time in between irradiation and measurement. Furthermore, for the cases that are affected by a contaminating reaction channel, another correction factor was introduced, taking this into account. The final formula for the activated nuclei experimental calculation is the following:

$$N_{act} = \frac{counts * corrections}{\epsilon I(1 - e^{-\lambda t_{meas}})e^{-\lambda t_{wait}}} \tag{4.4}$$

with

- I the γ-ray intensity
- λ the isotope's decay constant

The number of activated nuclei is of course related to the cross section of the reaction, via

$$N_{act} = SACS * N_T * \Phi * f_B \tag{4.5}$$

with

- N_T the number of target nuclei
- Φ the incident particle fluence

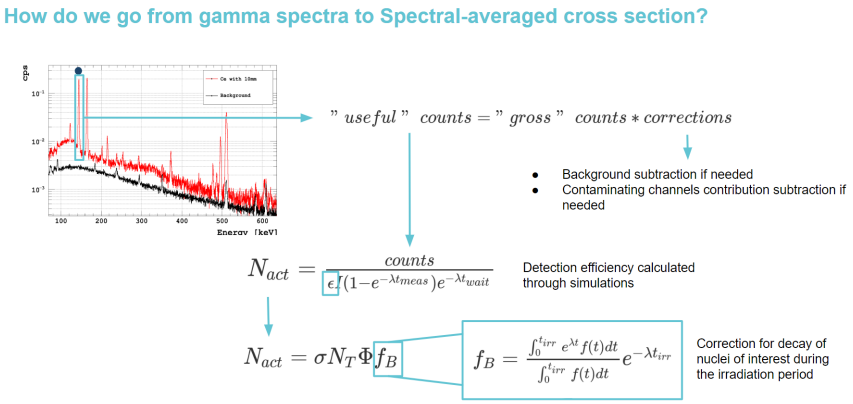

Figure 37: Schematic representation of the analysis procedure steps.

Having irradiated both a sample and a reference foil we can then extract the ratio of their SACS through

$$\frac{SACS_{sample}}{SACS_{ref}} = \frac{\frac{N_{act,sample}}{N_{T,sample}\Phi f_{b,sample}}}{\frac{N_{act,ref}}{N_{T,ref}\Phi f_{b,ref}}} = \frac{N_{act,sample} N_{T,ref} f_{b,ref}}{N_{act,ref} N_{T,sample} f_{b,sample}} \tag{4.6}$$

A schematic representation of this procedure can be found in Fig. 37

The experimental values for the SACS ratios between sample and reference foil can be found in table 11.

After having obtained the experimental results we need to assess two questions:

1. Do we have a good understanding of the procedures and good control of our data?

2. How do they compare to the objective of the study?

We address these questions below.

4.4.1 Simulated SACS ratios

In order to verify that we have good control over the whole procedure, we can test if our simulations satisfactorily reproduce the experimental results. If so, we can rely on the simulations for further studies.

Sample	B_4C thickness [mm]	SACS ratio	Spread (%)
Ge	5	0.0177	3
Ge	10	0.0214	3
Ge	15	0.0234	3
Ge	20	0.0246	3
Ce	5	0.0208	10
Ce	10	0.0286	10
Ce	15	0.0326	15
Ce	20	0.0372	15
Zr	5	0.0219	10
Zr	10	0.0331	10
Zr	15	0.0416	15
Zr	20	0.0382	15

Table 11: Experimentally calculated SACS ratios of sample over reference gold foil

To do that, we can calculate the same SACS ratios using the simulated neutron flux. We can fold the neutron energy distribution with each reaction's cross section, as described above for the (n,2n) competing channel contribution subtraction. We can do this for the sample as well as the reference foil and extract the simulated SACS ratios. Again, there will be a spread in the data because of the different available cross section evaluations.

4.4.2 SACS ratios with a Maxwellian beam

Now, if we calculate again the same ratios but this time instead of using the actual simulated NEAR beam we use the ideal Maxwellian neutron beam, we can extract what would be the ideal result of this study, the perfect beam shaping that would allow for MACS measurements at the NEAR station. By comparing our experimental results to these values, we can assess how far we are from the ideal case.

A comparison of all the above mentioned calculations can be found in Fig. 38, 39, 40.

The conclusions from this comparison and steps to improve will be discussed in the next chapter.

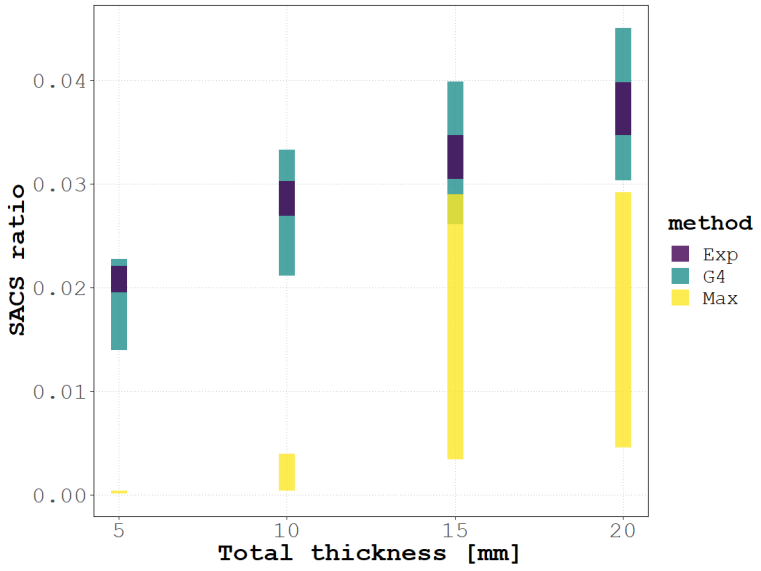

Figure 38: Comparison between experimental SACS ratios (purple), simulated ones using Geant4 (cyan) and ideal ones calculated with a Maxwellian beam (yellow) for Ce

5 Conclusions and discussion

The motivation behind this project is the fact that Maxwellian-averaged cross section (MACS) measurements play a critical role in nuclear astrophysics, as they can improve not only our understanding of the underlying nucleosynthesis processes but also the modelling of the chemical evolution of the universe. Many measurements of interest for MACS extraction can proceed via the time-of-flight technique, however, this technique is not always applicable (e.g. because of the small sample mass in radioactive samples). Additionally, in several physics cases the energy covered through tof measurements is not wide enough as to extract the MACS for the actual stellar temperatures of interest. In such cases, integral measurements can be an alternative solution.

This project was submitted to INTC, the CERN scientific committee responsible for reviewing experimental proposals for the ISOLDE and n_TOF facilities, in January 2022 and was subsequently approved during its meeting next month [68]. It aimed at investigating whether it is possible to shape the neutron flux of the NEAR station of the n_TOF facility into a

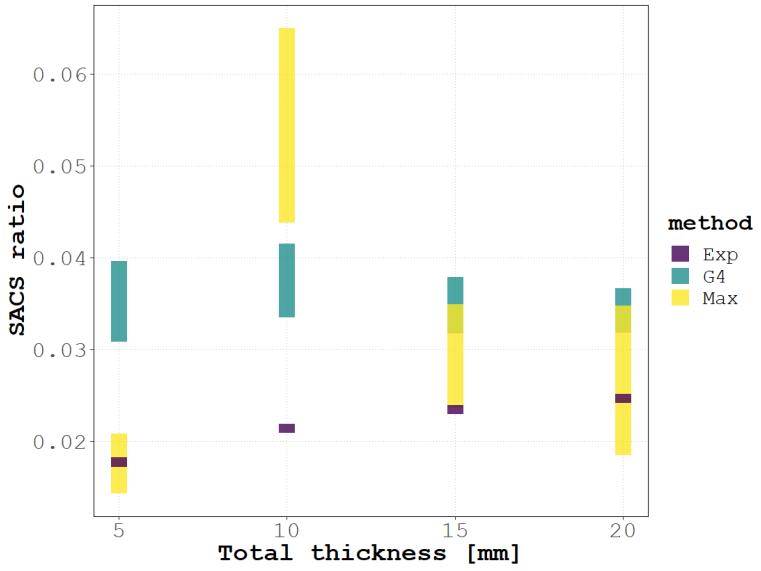

Figure 39: Comparison between experimental SACS ratios (purple), simulated ones using Geant4 (cyan) and ideal ones calculated with a Maxwellian beam (yellow) for Ge

Maxwell-Boltzmann distribution with the use of filters based on ^{10}B, a material that highly interacts with low energy neutrons, in order to perform integral MACS measurements. Neutron capture reactions with well known point-wise cross sections were chosen to be measured as part of this feasibility study. Four different thicknesses of filtering material were used in order to extract better quality conclusions.

The final results of this study are represented by Fig. 38, 39, 40 and the following conclusions can be extracted from them:

- High-accuracy SACS measurements are feasible even when minimal sample mass is available (depending on the cross section, even masses of the order of ngr can be considered).
- The deduction of MACS from the measured SACS can deviate by a factor of 2 or 3. Nevertheless, this is sufficient to "nail down" reaction cross section estimations based solely on theoretical calculations.

Even though the situation as-is leads to a maximum accuracy of a factor 2 to 3, depending on the physics case and cross section shape, it can be

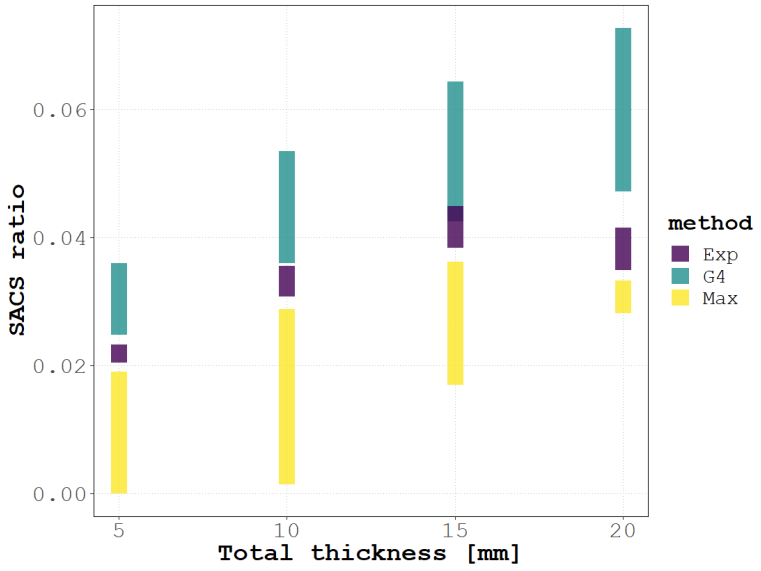

Figure 40: Comparison between experimental SACS ratios (purple), simulated ones using Geant4 (cyan) and ideal ones calculated with a Maxwellian beam (yellow) for Zr

useful for physics cases which have never been measured, or for which the MACS is known with a very high uncertainty. If theoretical calculation of the cross section can be performed, they can further improve this accuracy when combined with simulations of the filtering procedure.

As illustrated in the results figures, higher filter thicknesses lead to better agreement between SACS and MACS, as more resonances are filtered out. This can improve the current situation, up to a certain point, as too thick filters can introduce further problems, such as too much neutron scattering altering the results.

A safe method to increase the proximity of measured SACS to MACS is to introduce a moderating system before the NEAR activation station, so that the shape of the flux is further modified. Preliminary simulations of such a system performed by the n_TOF collaboration confirm this point.

6 APPENDIX

6.1 The activation technique equations

When irradiating a sample, the induced nuclear reactions lead to the production of new, activated, nuclei. The number of those activated nuclei, N_{act}, depends on the number of initial, target, nuclei in the sample, N_T, the reaction cross section, σ and the flux of incident particles, $f(t)$.

The rate at which the number of activated nuclei changes during the irradiation period, t_{irr}, is given by the following differential equation:

$$\frac{dN_{act}}{dt} = \sigma f(t)(N_T - N_{act}) - \lambda N_{act} \tag{6.1}$$

Because the number of target nuclei is much greater than the activated nuclei, we can consider that

$$N_T - N_{act} \approx N_T$$

and thus the differential equation can be written as follows:

$$\frac{dN_{act}}{dt} = \sigma f(t) N_T - \lambda N_{act} \tag{6.2}$$

Then:

$$\frac{dN_{act}}{dt} + \lambda N_{act} = \sigma f(t) N_T$$

$$\frac{dN_{act}}{dt} e^{\lambda t} + \lambda N_{act} e^{\lambda t} = \sigma f(t) N_T e^{\lambda t}$$

$$\frac{d}{dt}[N_{act} e^{\lambda t}] = \sigma f(t) N_T e^{\lambda t}$$

If we consider that we start the irradiation at $t = 0$ and finish at $t = t_{irr}$,

$$\int_0^{t_{irr}} \frac{d}{dt}[N_{act} e^{\lambda t}] dt = \int_0^{t_{irr}} \sigma f(t) N_T e^{\lambda t} dt$$

At the beginning of the irradiation, $N_{act} = 0$ so

$$N_{act} e^{\lambda t_{irr}} = \sigma N_T \int_0^{t_{irr}} f(t) e^{\lambda t} dt$$

In order to reach a more compact and convenient formula, we can multiply and divide by $\int_0^{t_{irr}} f(t)dt$:

$$N_{act} = \sigma N_T e^{-\lambda t_{irr}} \int_0^{t_{irr}} f(t)dt \frac{\int_0^{t_{irr}} f(t)e^{\lambda t}dt}{\int_0^{t_{irr}} f(t)dt} = \sigma N_T e^{-\lambda t_{irr}} \Phi \frac{\int_0^{t_{irr}} f(t)e^{\lambda t}dt}{\int_0^{t_{irr}} f(t)dt}$$

or

$$N_{act} = \sigma N_T \Phi f_B \tag{6.3}$$

with

$$f_B = \frac{\int_0^{t_{irr}} e^{\lambda t} f(t)dt}{\int_0^{t_{irr}} f(t)dt} e^{-\lambda t_{irr}}$$

a correction factor representing the nuclei that decay during the irradiation period. More details on the theoretical extraction and experimental calculation of the f_B correction factor can be found in 6.2

If we consider that the measurement starts after a time t_{wait} has elapsed since the end of the irradiation, the number of nuclei of interest at the beginning of the measurement are

$$N_0 = N_{act} e^{-\lambda t_{wait}} \tag{6.4}$$

The rate at which our detector records counts is given by

$$cps = \frac{dN}{dt} \epsilon I \tag{6.5}$$

with *cps* the "counts per second" we record, $\frac{dN}{dt}$ the decay rate of the activated nuclei, ϵ the detection efficiency and I the intensity of the emitted radiation.

According to the decay law,

$$\frac{dN}{dt} = \lambda N$$

and

$$N = N_0 e^{-\lambda t}$$

Hence the counting rate is given by

$$cps = \epsilon I \lambda N_{act} e^{-\lambda t_{wait}} e^{-\lambda t} \tag{6.6}$$

If we consider that the measurement lasts for t_{meas}, the total number of counts recorder are calculated as

$$counts = \epsilon I \lambda N_{act} e^{-\lambda t_{wait}} \int_0^{t_{meas}} e^{-\lambda t} =$$

$$\epsilon I \lambda N_{act} e^{-\lambda t_{wait}} \frac{1}{-\lambda} (e^{-\lambda t_{meas}} - 1) =$$

$$\epsilon I N_{act} e^{-\lambda t_{wait}} (1 - e^{-\lambda t_{meas}})$$

And if we substitute the activated nuclei as calculated in 6.3,

$$counts = \epsilon I N_T \sigma \Phi f_B e^{-\lambda t_{wait}} (1 - e^{-\lambda t_{meas}}) \tag{6.7}$$

We can solve the above equation for any variable that is unknown in the case of each specific experiment, for example the cross-section

$$\sigma = \frac{counts * corrections}{\Phi \epsilon I N_T e^{-\lambda t_{wait}} \left(1 - e^{-\lambda t_{meas}}\right) f_B} \tag{6.8}$$

or the incident particle flux

$$\Phi = \frac{counts * corrections}{\sigma \epsilon I N_T e^{-\lambda t_{wait}} \left(1 - e^{-\lambda t_{meas}}\right) f_B} \tag{6.9}$$

6.2 The f_b correction factor

As discussed in 6.1, we need a correction factor accounting for the nuclei of interest that were produced but decayed during the irradiation time so they could not be recorded in the experimental spectra. This correction factor, the f_B correction factor, is given by:

$$f_B = \frac{\int_0^{t_{irr}} e^{\lambda t} f(t)dt}{\int_0^{t_{irr}} f(t)dt} e^{-\lambda t_{irr}} \tag{6.10}$$

In case the incident particle beam is constant with time, 6.10 can easily be solved analytically and provide the correction factor as:

$$f_B = \frac{\int_0^{t_{irr}} e^{\lambda t} f(t)dt}{\int_0^{t_{irr}} f(t)dt} e^{-\lambda t_{irr}} =$$

$$= \frac{\Phi \int_0^{t_{irr}} e^{\lambda t} dt}{\Phi \int_0^{t_{irr}} dt} e^{-\lambda t_{irr}}$$

$$= \frac{\frac{1}{\lambda}(e^{\lambda t_{irr}} - 1)}{t_{irr}} e^{-\lambda t_{irr}}$$

And finally

$$f_B = \frac{1 - e^{-\lambda t_{irr}}}{\lambda t_{irr}} \tag{6.11}$$

In reality, it is very probable that the incident particle beam is not constant. In that case, we need to substitute the integral with a sum and proceed with a bin-by-bin calculation.

$$f_B = \frac{\sum_{low}^{upper} e^{\lambda t} f(t)\Delta t}{\sum_{low}^{upper} f(t)\Delta t} e^{-\lambda t_{irr}} \tag{6.12}$$

For this bin-by-bin calculation, the following code in C++ was developed:

```
//=======================================//
//   Code to extract the fB correction   //
//   factor from TIMBER data grouped in  //
//   specific time intervals             //
//                                M.E.S. //
//=======================================//

void fb() {
cout<<endl;

//===============================================//
//                  USER INPUT                   //
//                --------------                 //
// Half-lif of isotope in seconds                //
double t12 = 15.31*24*60*60;                     //
// Irradiation time in seconds                   //
double tirr = 1.883580e+06;                      //
// Time grouped in seconds                       //
double group = 100;                              //
// Name of TIMBER .csv file                      //
string name = "TIMBER_data_MAM1";                //
//===============================================//


  //==== Calculate decay constant etc
  double lambda = log(2)/t12;
  double eltirr = exp(-lambda*tirr);

  //==== Open file and get irradiation history histogram
  // (henceforth denoted as histogry)
  string location = "/eos/user/m/mastamat/NEAR/IrrHistory
     ↪ /";
  string filename = location+name+Form("_grouped_%.0fs.
     ↪ root",group);
  TFile *fin = new TFile(Form("%s", filename.c_str()));
  TH1F *h_history = (TH1F*)fin->Get("h_history");

  //==== Plot histogry
  TCanvas *ch =
  new TCanvas("ch", Form("Histogram␣grouped␣by␣%.0fs",
     ↪ group));
  ch->cd();
  h_history->Draw("HIST");
  h_history->GetYaxis()->SetMaxDigits(3);
```

```
  //==== Calculate fB
  int bins = h_history->GetNbinsX();
  double dt = group;
  double integral_num=0, integral_denom=0;

  for (int i=1; i<bins+1; i++) {
    integral_num += (h_history->GetBinContent(i)*1.e10 *
        ↪ (exp(lambda*dt*i) - exp(lambda*dt*(i-1)) ) )/
        ↪ lambda;
    integral_denom += h_history->GetBinContent(i)*1.e10 *
        ↪ dt;
  }//...for loop in bins

  double fb = integral_num/integral_denom * eltirr;

  //==== Print information
  cout<<endl<<"Correction␣factor␣fb␣=␣"<<fb;
  cout<<"and␣if␣you␣needed␣1/fb␣=␣"<<1./fb<<endl<<endl;

}//...the end
```

6.3 The data analysis code

Data analysis was mainly performed using the following code in C++. The user needs to prepare 3 input files, the first being the irradiation runbook containing all irradiation information such as beginning and end date and time, number of protons, etc, the second being a summary of the decay characteristics of each nuclei of interest (gamma-ray energy, intensity, HPGe efficiency at that energy, etc) and the third being the HPGe detector energy calibration parameters. After that, the user can execute the analysis code, providing as arguments the element of interest, the filter thickness of interest, whether the analysis will refer to the sample of the reference foil, which gamma-ray from the decay scheme will be studied and which data file will be used (the data file is the file resulting from the data acquisition system of use). The code then proceeds to calculate the parameters needed (for example irradiation, waiting and measuring time, the number of net counts in the photopeak of interest, etc) for the final result, which is the number of activated nuclei of interest at the end of the irradiation period.

```
#include <string.h>
#include <fstream>
#include <iostream>

// ROOT Headers
#include "TSystem.h"
#include "TROOT.h"
#include "TH1I.h"
#include "TFile.h"
#include "TTree.h"
#include "TBranch.h"
#include "TCanvas.h"
#include "TColor.h"
#include "TLegend.h"
#include "TPad.h"
#include "TString.h"
#include "TObject.h"
#include "TStyle.h"

using namespace std;

#define BOLDGREEN   "\033[1m\033[32m"      /* Bold Green
   ↪ */
#define BOLDCYAN    "\033[1m\033[36m"      /* Bold Cyan
   ↪ */
```

```
#define BOLDWHITE   "\033[1m\033[37m"      /* Bold White
   ↪ */
#define BOLDYELLOW  "\033[1m\033[33m"      /* Bold Yellow
   ↪  */
#define RESET       "\033[0m"


//=== External functions declaration
TTree *IrradiationData();
TTree *GammaData();
TTree *MeasData(string, int, TString*, int);
TTree *CountsData(TH1F *, double);

//==================================//
//          MAIN FUNCTION           //
//==================================//

void analyse(string elmnt, int thickness, char
   ↪ sample_or_ref, int g_indx, int file) {

  //----------------------------- RETRIEVING INFORMATION
     ↪ ------------------------------//

  //==== Get irradiation information tree
  TTree *IrradiationTree = IrradiationData();
  int irradiations = IrradiationTree->GetEntries();
  // Variables needed
  TString *element=0, *sampleID=0, *RefAuID=0;
  int B4C;
  TDatime *DTIrrStart=0, *DTIrrStop=0;
  double protons, fbSamp, fbRef;

  //===== Get the entry that matches the element and the
     ↪ thickness you want
  IrradiationTree->Draw("Entry$>>hist(irradiations,0,
     ↪ irradiations)", Form("element==\"%s\"␣&&␣B4C==%d"
     ↪ , elmnt.c_str(), thickness), "goff");
  TH1I *hist = (TH1I*)gDirectory->Get("hist");
  int irrEntry = hist->GetBinLowEdge(hist->
     ↪ FindFirstBinAbove(0));
  delete hist;

  //===== Save irradiation data
  IrradiationTree->SetBranchAddress("element",&element);
```

```
IrradiationTree->SetBranchAddress("sampleID", &sampleID
   ↪ );
IrradiationTree->SetBranchAddress("RefAuID", &RefAuID);
IrradiationTree->SetBranchAddress("B4C", &B4C);
IrradiationTree->SetBranchAddress("DTstart", &
   ↪ DTIrrStart);
IrradiationTree->SetBranchAddress("DTstop", &DTIrrStop)
   ↪ ;
IrradiationTree->SetBranchAddress("protons", &protons);
IrradiationTree->SetBranchAddress("fbSamp", &fbSamp);
IrradiationTree->SetBranchAddress("fbRef", &fbRef);
IrradiationTree->GetEntry(irrEntry);

double tirr = (DTIrrStop->Convert() - DTIrrStart->
   ↪ Convert());

//ooooooooooooooooooooooooooooooo

//==== Get gamma rays information tree
TTree *GammaTree = GammaData();
int gammas = GammaTree->GetEntries();
// Variables needed
TString *element2=0;
int g_index;
double halflife, energy, intensity, efficiency;
//===== Get the entry that matches the element and the
   ↪ thickness you want
if (sample_or_ref=='s') GammaTree->Draw("Entry$>>hist(
   ↪ gammas,0,gammas)", Form("element2==\"%s\"␣&&␣
   ↪ g_index==%d", elmnt.c_str(), g_indx), "goff");
if(sample_or_ref=='r')  GammaTree->Draw("Entry$>>hist(
   ↪ gammas,0,gammas)", Form("element2==\"Au\"␣&&␣
   ↪ g_index==%d", g_indx), "goff");
hist = (TH1I*)gDirectory->Get("hist");
int gammaEntry = hist->GetBinLowEdge(hist->
   ↪ FindFirstBinAbove(0));
delete hist;
//===== Save gamma ray data
GammaTree->SetBranchAddress("element2",&element2);
GammaTree->SetBranchAddress("g_index", &g_index);
GammaTree->SetBranchAddress("halflife", &halflife);
GammaTree->SetBranchAddress("energy", &energy);
GammaTree->SetBranchAddress("intensity", &intensity);
GammaTree->SetBranchAddress("efficiency", &efficiency);
GammaTree->GetEntry(gammaEntry);
```

```
 //ooooooooooooooooooooooooooooooo

 //==== Get Measurement information tree
 TTree *MeasTree;
back:
 if (sample_or_ref == 's') MeasTree = MeasData(elmnt,
    ↪ thickness, sampleID, file);
 if (sample_or_ref == 'r') MeasTree = MeasData(elmnt,
    ↪ thickness, RefAuID, file);
 if (sample_or_ref != 's' && sample_or_ref != 'r') {cout
    ↪ <<"You␣want␣me␣to␣analyse␣the␣sample␣or␣the␣
    ↪ reference␣foil?"<<endl<<"Type␣s␣or␣r:␣"; cin>>
    ↪ sample_or_ref; goto back;}
 // Variables needed
 TH1F *h_energy_counts=0; TH1F *h_channels_counts=0;
 double tmeas=0;
 TDatime *DTMeasStart=0;
 //==== Get the only entry existing since it's just on
    ↪ one file
 MeasTree->SetBranchAddress("DTMeasStart", &DTMeasStart)
    ↪ ;
 MeasTree->SetBranchAddress("livetime", &tmeas);
 MeasTree->SetBranchAddress("h_energy_counts", &
    ↪ h_energy_counts);
 MeasTree->SetBranchAddress("h_channels_counts", &
    ↪ h_channels_counts);
 MeasTree->GetEntry(0);

 //ooooooooooooooooooooooooooooooo

 //==== GetCounts information tree
 TTree *CountsTree = CountsData(h_energy_counts, energy)
    ↪ ;
 // Variables needed
 double counts, error;
 //==== Get the only entry existing
 CountsTree->SetBranchAddress("counts", &counts);
 CountsTree->SetBranchAddress("error", &error);
 CountsTree->GetEntry(0);

 //-------------------------------------- CALCUATIONS
    ↪ ----------------------------------------//

 //===== Calculate useful values
```

```
double lambda = log(2)/halflife;
double twait = DTMeasStart->Convert()-DTIrrStop->
   ↪ Convert();
double eltmeas = exp(-lambda*tmeas);
double eltwait = exp(-lambda*twait);

//==== Calculate number of activated nuclei etc
double Nact = counts / (efficiency * intensity *
   ↪ eltwait * (1-eltmeas) ) ;
double Aeoi = lambda * Nact ;
double Asat = Nact / (fbSamp*tirr) ;


//---------------------------------- PLOTTING THE
   ↪ SPECTRUM ----------------------------------//

TCanvas *cspec = new TCanvas("cspec");
cspec->cd(); gPad->SetLogy();
h_energy_counts->GetXaxis()->SetRange(1,
   ↪ h_energy_counts->GetNbinsX()); h_energy_counts->
   ↪ Draw();
gPad->BuildLegend();


//------------------------------ PRINTING INFORMATION
   ↪ ON SCREEN ------------------------------//

//===== Print relevant irradiation information
cout<<BOLDYELLOW<<endl<<"************************␣
   ↪ General␣Information␣**********************"<<endl
   ↪ ;
cout<<BOLDGREEN;
cout<<"Experiment␣Information:"<<endl<<"
   ↪ -------------------------"<<endl;
cout<<"Element:␣"<<BOLDCYAN<<*element<<BOLDGREEN<<endl
   ↪ <<"B4C␣thickness␣[mm]:␣"<<BOLDCYAN<<B4C<<
   ↪ BOLDGREEN<<endl;
cout<<"Sample␣ID:␣"<<BOLDCYAN<<*sampleID<<BOLDGREEN<<"␣
   ↪ and␣Reference␣gold␣ID:␣"<<BOLDCYAN<<*RefAuID<<
   ↪ BOLDGREEN<<endl;
cout<<RESET<<endl;

//===== Print relevant gamma-rays/physics information
cout<<BOLDGREEN<<"Physics␣information:"<<endl<<"
   ↪ ---------------------"<<endl;
```

```
cout<<"Half-life␣of␣product␣[s]:␣"<<BOLDCYAN<<halflife
    ↪ <<BOLDGREEN<<endl;
cout<<"Emmitted␣g-ray␣energy␣[keV]:␣"<<BOLDCYAN<<energy
    ↪ <<BOLDGREEN<<endl;
cout<<"Emmitted␣g-ray␣intensity:␣"<<BOLDCYAN<<intensity
    ↪ <<BOLDGREEN<<endl;
cout<<"Efficiency␣@␣"<<energy<<"␣keV:␣"<<BOLDCYAN<<
    ↪ efficiency<<BOLDGREEN<<endl;
cout<<RESET<<endl;

//===== Print relevant irradiation information
cout<<BOLDGREEN<<"Irradiation␣information:"<<endl<<"
    ↪ ------------------------"<<endl;
cout<<BOLDGREEN<<"Irradiation␣lasted␣from:␣"<<BOLDCYAN
    ↪ <<DTIrrStart->AsString()<<BOLDGREEN<<"␣to␣"<<
    ↪ BOLDCYAN<<DTIrrStop->AsString()<<BOLDGREEN<<endl;
cout<<"Irradiation␣time␣[s]:␣"<<BOLDCYAN<<tirr<<
    ↪ BOLDGREEN<<endl;
cout<<"Total␣protons:␣"<<BOLDCYAN<<protons<<BOLDGREEN<<
    ↪ endl;
cout<<"fb␣for␣"<<elmnt<<":␣"<<BOLDCYAN<<fbSamp<<
    ↪ BOLDGREEN<<"␣and␣for␣the␣reference␣foil:␣"<<
    ↪ BOLDCYAN<<fbRef<<BOLDGREEN<<endl;
cout<<RESET<<endl;

//==== Print relevant measurement information
cout<<BOLDGREEN<<"Activity␣measurement␣information:"<<
    ↪ endl<<"---------------------------------"<<endl;
cout<<"Measurement␣started:␣"<<BOLDCYAN<<DTMeasStart->
    ↪ AsString()<<BOLDGREEN<<endl;
cout<<"Waiting␣time␣[s]:␣"<<BOLDCYAN<<twait<<BOLDGREEN
    ↪ <<endl;
cout<<"␣␣␣exp(-ltwait):␣"<<BOLDCYAN<<eltwait<<BOLDGREEN
    ↪ <<endl;
cout<<"Measuring␣time␣[s]:␣"<<BOLDCYAN<<tmeas<<
    ↪ BOLDGREEN<<endl;
cout<<"␣␣␣exp(-ltmeas):␣"<<BOLDCYAN<<eltmeas<<BOLDGREEN
    ↪ <<endl;
cout<<RESET<<endl;

//===== Print results
cout<<BOLDYELLOW<<endl<<"**********␣
    ↪ Calculation␣results␣**********"<<endl
    ↪ ;
```

```
  cout<<BOLDGREEN<<"Counts␣in␣photopeak:␣"<<BOLDCYAN<<
     ↪ counts<<BOLDGREEN<<"␣+-␣"<<BOLDCYAN<<error<<
     ↪ BOLDGREEN<<endl;
  cout<<"Number␣of␣activated␣nuclei:␣"<<BOLDCYAN<<Nact<<
     ↪ BOLDGREEN<<endl;
  cout<<"Activity␣Aeoi␣[Bq]:␣"<<BOLDCYAN<<Aeoi<<BOLDGREEN
     ↪ <<endl;
  cout<<"Saturation␣activity␣[Bq]:␣"<<BOLDCYAN<<Asat<<
     ↪ BOLDGREEN<<endl;
  cout<<RESET<<endl;


  cout<<endl;
}//...the end

//=====================================//

//=================================//
//        EXTERNAL FUNCTIONS       //
//=================================//

//---------------------------------//
//----- Read irradiation data -------//

TTree *IrradiationData(){

  // Irradiation history file
  string IrradiationFilename = "/eos/user/m/mastamat/NEAR
     ↪ /PracticalInformation/IrradiationHistory.txt";
  ifstream IrradiationInfile(IrradiationFilename.c_str())
     ↪ ;
  // Get number of lines of the file (number of
     ↪ irradiations)
  const int lines = (gSystem->GetFromPipe(Form("wc␣-l␣<␣%
     ↪ s",IrradiationFilename.c_str()))).Atoi();

  // Variables needed
  TString element, sampleID, RefAuID;
  string start_date, start_time, stop_date, stop_time;
  int B4C;
  TDatime DTstart, DTstop;
  double protons, fbSamp, fbRef;

  // Create a Tree
```

```
  TTree *IrradiationTree = new TTree("IrradiationTree", "
     ↪ Irradiation␣data");
  IrradiationTree->Branch("element",&element);
  IrradiationTree->Branch("sampleID", &sampleID);
  IrradiationTree->Branch("RefAuID", &RefAuID);
  IrradiationTree->Branch("B4C", &B4C);
  IrradiationTree->Branch("DTstart", &DTstart);
  IrradiationTree->Branch("DTstop", &DTstop);
  IrradiationTree->Branch("protons", &protons);
  IrradiationTree->Branch("fbSamp", &fbSamp);
  IrradiationTree->Branch("fbRef", &fbRef);

  // Read file and store information in said tree
  for (int i=0; i<lines; i++) {
    if (IrradiationInfile.peek()=='#') IrradiationInfile.
       ↪ ignore(1000, '\n');
    else {
      IrradiationInfile>>element>>sampleID>>RefAuID>>B4C
         ↪ >>start_date>>start_time>>stop_date>>
         ↪ stop_time>>protons>>fbSamp>>fbRef;
      string start_temp = start_date+"␣"+start_time;
         ↪ string stop_temp = stop_date+"␣"+stop_time;
      DTstart = TDatime(start_temp.c_str()); DTstop =
         ↪ TDatime(stop_temp.c_str());
      IrradiationTree->Fill();
      //cout<<i<<"  "<<DTstart.AsString()<<"  "<<DTstop.
         ↪ AsString()<<endl;
    }//...if line is useful (doesn't start with a #)
  }//...while reading file

  return IrradiationTree;

}//... End of reading irradiation data

//----- Read irradiation data -------//
//-----------------------------------//


//-----------------------------------//
//------ Read gamma-ray data --------//

TTree *GammaData(){

  // Gamma-rays and related info file
```

```
  string GammaFilename = "/eos/user/m/mastamat/NEAR/
     ↪ PracticalInformation/grays.txt";
  ifstream GammaInfile(GammaFilename.c_str());
  // Get number of lines of the file
  const int lines = (gSystem->GetFromPipe(Form("wc␣-l␣<␣%
     ↪ s",GammaFilename.c_str()))).Atoi();

  // Variables needed
  TString element2;
  int g_index;
  double halflife, energy, intensity, efficiency;

  // Create a Tree
  TTree *GammaTree = new TTree("GammaTree", "Gamma␣data")
     ↪ ;
  GammaTree->Branch("element2",&element2);
  GammaTree->Branch("g_index", &g_index);
  GammaTree->Branch("halflife", &halflife);
  GammaTree->Branch("energy", &energy);
  GammaTree->Branch("intensity", &intensity);
  GammaTree->Branch("efficiency", &efficiency);

  // Read file and store information in said tree
  for (int i=0; i<lines; i++) {
    if (GammaInfile.peek()=='#') GammaInfile.ignore(1000,
       ↪  '\n');
    else {
      GammaInfile>>element2>>halflife>>g_index>>energy>>
         ↪ intensity>>efficiency;
      GammaTree->Fill();
      //cout<<i<<"  "<<DTstart.AsString()<<"  "<<DTstop.
         ↪ AsString()<<endl;
    }//...if line is useful (doesn't start with a #)
  }//...while reading file

  return GammaTree;

}//... End of reading gamma-ray data

//------ Read gamma-ray data --------//
//-------------------------------------//


//-------------------------------------//
//----- Read measurement file -------//
```

```
TTree *MeasData(string element, int thickness, TString*
   ↪ sample_temp, int file) {

  //=== Variables
  double content;
  string word;
  string start_date, start_time;
  double live_time;
  char dummy;
  TDatime DTstart;
  TH1F *h_energy_counts;

  //==== Tree with data
  TTree *MeasTree = new TTree("MeasurementData", "
     ↪ Measurement␣Data");
  MeasTree->Branch("DTMeasStart", &DTstart);
  MeasTree->Branch("livetime", &live_time);

  //=== Checkpoints
  double channels = 8192;
  string keyword_time = "LIVE_TIME";
  string keyword_start = "START_TIME";
  string keyword_data = "<<DATA>>";

  //=== Read measurement and calibration file
  string sample(sample_temp->Data());
  string location = "/eos/user/m/mastamat/NEAR/
     ↪ MeasurementFiles/";
  string folder = element + to_string(thickness) + "mm/";
  string namebase = sample + "_9cm_File" + to_string(file
     ↪ );
  string suffix = ".mca";
  string filename = location + folder + namebase + suffix
     ↪ ;
  cout<<filename<<endl;

  //=== Read file and save start date and time
  ifstream in(filename);
  while(in>>word) {
     if (word==keyword_time) in>>dummy>>live_time; //If
        ↪ you reach LIVE TIME save the value
     if (word==keyword_start) {in>>dummy>>start_date>>
        ↪ start_time; break;}
  }
```

```
string start_tot = start_date + "␣" + start_time;
string sday = "00"; sday[0]=start_tot[3]; sday[1]=
   ↪ start_tot[4];
string smonth = "00"; smonth[0]=start_tot[0]; smonth
   ↪ [1]=start_tot[1];
string syear = "0000"; syear[0]=start_tot[6]; syear[1]=
   ↪ start_tot[7]; syear[2]=start_tot[8]; syear[3]=
   ↪ start_tot[9];
string date = syear+"-"+smonth+"-"+sday;
string for_dt = date+"␣"+start_time;
DTstart = TDatime(for_dt.c_str());

//=== Read calibration file
double a=1., b=1.;
string calidate_low, calidate_up;
ifstream incali("/eos/user/m/mastamat/NEAR/
   ↪ PracticalInformation/Calibration.txt");
int dbg=0;
while(!incali.eof()) {
  if (incali.peek()=='#') incali.ignore(1000, '\n');
  else {
    dbg++;
    incali>>calidate_low>>calidate_up>>a>>b;
    string temp_low = calidate_low + "␣10:00:00";
    string temp_up = calidate_up + "␣10:00:00";
    TDatime dtlow(temp_low.c_str()); TDatime dtup(
       ↪ temp_up.c_str());
    //cout<<dbg<<"  "<<calidate_low<<"  "<<dtlow.
       ↪ Convert()<<"  "<<DTstart.Convert()<<"  "<<
       ↪ dtup.Convert()<<"  "<<calidate_up<<endl;
    if (dtlow.Convert() < DTstart.Convert() && DTstart.
       ↪ Convert() < dtup.Convert() ) {/*cout<<"***"<<
       ↪ dbg<<endl;*/break;}
  }//...if useful line
}

//cout<<"a "<<a<<endl<<"b "<<b<<endl;

//=== Histogram declaration
double low = a;
double high = a+b*(channels-1);
string titledate = "␣-␣" +  sday +"." + smonth + "." +
   ↪ syear;
string name = sample_temp->Data() + titledate;
```

```
  TH1F *h_channels_counts = new TH1F("h_channels_counts",
     ↪  Form("%s;Channel;Counts", name.c_str()),
     ↪ channels, 0, channels);
  h_energy_counts = new TH1F("h_energy_counts", Form("%s;
     ↪ Energy␣[keV];Counts", name.c_str()), channels,
     ↪ low, high);

  MeasTree->Branch("h_channels_counts", "TH1F", &
     ↪ h_channels_counts, 32000, 0);
  MeasTree->Branch("h_energy_counts", "TH1F",  &
     ↪ h_energy_counts, 32000, 0);

  //==== Read file and save data
  while(in>>word) {
     if (word==keyword_data) break; //If you reach <<DATA
        ↪ >> stop
  }//...while
  for (int i=0; i<channels; i++) {
     in>>content;
     h_channels_counts->SetBinContent(i+1, content);
     h_energy_counts->SetBinContent(i+1, content);
  }//...for

  MeasTree->Fill();

  return MeasTree;

}//... End of getting measurement information

//----- Read measurement file -------//
//-----------------------------------//



//-----------------------------------//
//--------- Getting counts ----------//

TTree *CountsData(TH1F* h, double energy) {

  //=== Create canvas and zoom
  int zoom_low = h->FindBin(energy) - 150;
  int zoom_up  = h->FindBin(energy) + 150;

  TCanvas *cspec = new TCanvas("cspec", "cspec", 1000,
     ↪ 500);
```

```
cspec->Flush();
cspec->cd(); gPad->SetLogy();
h->GetXaxis()->SetRange(zoom_low, zoom_up); h->
   ↪ SetNdivisions(620);
h->Draw();
gPad->BuildLegend();
cspec->Update();

// Variables
double low, up;
double background;
double net_area, error;
int bg_channels;

TTree *CountsTree = new TTree("CountsTree", "Counts␣in␣
   ↪ photopeak");
CountsTree->Branch("counts", &net_area);
CountsTree->Branch("error", &error);

while (true) {
  cout<<endl<<"Lower␣limit␣for␣peak␣counting:␣"; cin>>
     ↪ low;
  cout<<"Upper␣limit␣for␣peak␣counting:␣"; cin>>up;
  cout<<"Number␣of␣background␣channels:␣"; cin>>
     ↪ bg_channels;

  //=== Find the channels belonging to low and up edges
  int ch_low = h->FindBin(low);
  int ch_up = h->FindBin(up);

  //=== Find the limits for the background evaluation
  int ch_start = ch_low - bg_channels;
  int ch_stop = ch_up + bg_channels;

  //=== Find the number of channels belonging to the
     ↪ peak
  int peak_ch = ch_up - ch_low + 1;

  //=== Calculate the net area
  double backav = ( h->Integral(ch_start, ch_low-1) + h
     ↪ ->Integral(ch_up+1, ch_stop) ) / (2*bg_channels
     ↪ );
  double background = peak_ch * backav;
  double gross_area = h->Integral(ch_low, ch_up);
  net_area = gross_area - background;
```

```
    error = sqrt(net_area + background*(1+peak_ch/(2*
       ↪ bg_channels) ) );

    //=== Draw
    TLine *llow = new TLine(low, backav/2, low, backav*2)
       ↪ ; llow->SetLineWidth(2); llow->SetLineColor(
       ↪ kRed); llow->Draw("SAME");
    TLine *lup = new TLine(up, backav/2, up, backav*2);
       ↪ lup->SetLineWidth(2); lup->SetLineColor(kRed);
       ↪ lup->Draw("SAME");
    TLine *lav = new TLine(low, backav, up, backav); lav
       ↪ ->SetLineWidth(2); lav->SetLineColor(kOrange);
       ↪ lav->Draw("SAME");
    cspec->Update();

    char satisfaction = 'n';
    cout<<endl<<"Are␣you␣satisfied␣with␣your␣intervals?␣(
       ↪ y/n)␣"; cin>>satisfaction;
    if (satisfaction=='y') {cspec->Close(); break;}

  }//...while

  CountsTree->Fill();
  return CountsTree;

}//...end of counts calculation

//--------- Getting counts ----------//
//-----------------------------------//
```

References

[1] Claus. E Rolfs and William S. Rodney. *Cauldrons in the Cosmos*. 1st. University of Chicago Press, 2005.

[2] Ian J. Thompson and Filomena M. Nunes. *Nuclear reaction for astrophysics*. Cambridge University Press, 2009.

[3] A Heger et al. "Massive star evolution: nucleosynthesis and nuclear reaction rate uncertainties". In: *New Astronomy Reviews* 46 (8-10 July 2002), pp. 463–468. ISSN: 13876473. DOI: 10.1016/S1387-6473(02)00184-7.

[4] Jean Audouze and Sylvie Vauclair. *An Introduction to Nuclear Astrophysics*. Vol. 18. D. Reidel Publishing Company, 1980.

[5] J. Yang et al. "Primordial nucleosynthesis - A critical comparison of theory and observation". In: *The Astrophysical Journal* 281 (June 1984), p. 493. ISSN: 0004-637X. DOI: 10.1086/162123.

[6] Gary Steigman, David N. Schramm, and James E. Gunn. "Cosmological limits to the number of massive leptons". In: *Physics Letters B* 66 (2 Jan. 1977), pp. 202–204. ISSN: 03702693. DOI: 10.1016/0370-2693(77)90176-9.

[7] Amanda I. Karakas and John C. Lattanzio. "The Dawes Review 2: Nucleosynthesis and Stellar Yields of Low- and Intermediate-Mass Single Stars". In: *Publications of the Astronomical Society of Australia* 31 (July 2014), e030. ISSN: 1323-3580. DOI: 10.1017/pasa.2014.21.

[8] Friedrich-Karl Thielemann, Ken'ichi Nomoto, and Masa-Aki Hashimoto. "Core-Collapse Supernovae and Their Ejecta". In: *The Astrophysical Journal* 460 (Mar. 1996), p. 408. ISSN: 0004-637X. DOI: 10.1086/176980.

[9] Harriet L. Dinerstein. "Observing the signatures of AGB s-process nucleosynthesis in planetary nebulae: An origins story". In: *Frontiers in Astronomy and Space Sciences* 9 (Dec. 2022). ISSN: 2296-987X. DOI: 10.3389/fspas.2022.1063995.

[10] E. Margaret Burbidge et al. "Synthesis of the Elements in Stars". In: *Reviews of Modern Physics* 29 (4 Oct. 1957), pp. 547–650. ISSN: 0034-6861. DOI: 10.1103/RevModPhys.29.547.

[11] F Kappeler, H Beer, and K Wisshak. "s-process nucleosynthesis-nuclear physics and the classical model". In: *Reports on Progress in Physics* 52 (8 Aug. 1989), pp. 945–1013. ISSN: 0034-4885. DOI: 10.1088/0034-4885/52/8/002.

[12] Aruna Goswami. "Nucleosynthesis in low-mass stars: Shedding light on the cosmic origin of heavy elements". In: *EPJ Web of Conferences* 297 (June 2024), p. 01004. ISSN: 2100-014X. DOI: 10.1051/epjconf/202429701004.

[13] S. Cristallo et al. "Evolution, nucleosynthesis, and yields of AGB stars at different metallicities. III. intermediate-mass models, revised low-mass models, and the pH-fruity interface". In: *The Astrophysical Journal Supplement Series* 219 (2 Aug. 2015), p. 40. ISSN: 1538-4365. DOI: 10.1088/0067-0049/219/2/40.

[14] G Cescutti et al. "Uncertainties in s-process nucleosynthesis in low-mass stars determined from Monte Carlo variations". In: *Monthly Notices of the Royal Astronomical Society* 478 (3 Aug. 2018), pp. 4101–4127. ISSN: 0035-8711. DOI: 10.1093/mnras/sty1185.

[15] N. Nishimura et al. "Uncertainties in s-process nucleosynthesis in massive stars determined by Monte Carlo variations". In: *Monthly Notices of the Royal Astronomical Society* 469 (2 Aug. 2017), pp. 1752–1767. ISSN: 0035-8711. DOI: 10.1093/mnras/stx696. URL: https://academic.oup.com/mnras/article-lookup/doi/10.1093/mnras/stx696.

[16] S. E. Woosley, A. Heger, and T. A. Weaver. "The evolution and explosion of massive stars". In: *Reviews of Modern Physics* 74 (4 Nov. 2002), pp. 1015–1071. ISSN: 0034-6861. DOI: 10.1103/RevModPhys.74.1015.

[17] Franz Kappeler. "The Origin of the Heavy Elements: The s Process". In: *Progress in Particle and Nuclear Physics* 43 (1999), pp. 419–483.

[18] F. Käppeler et al. "The s-process: Nuclear physics, stellar models, and observations". In: *Reviews of Modern Physics* 83 (1 Apr. 2011), pp. 157–193. ISSN: 0034-6861. DOI: 10.1103/RevModPhys.83.157.

[19] H. Beer and F. Käppeler. "Neutron capture cross sections on 138 Ba , 140,142 Ce , 175,176 Lu , and 181 Ta at 30 keV: Prerequisite for investigation of the 176 Lu cosmic clock". In: *Physical Review C* 21 (2 Feb. 1980), pp. 534–544. ISSN: 0556-2813. DOI: 10.1103/PhysRevC.21.534.

[20] W. Ratynski and F. Käppeler. "Neutron Capture Cross Section of ^{197}Au: A Standard for Stellar Nucleosynthesis". In: *Physical Review C* 37 (2 Feb. 1988), pp. 595–604. ISSN: 0556-2813. DOI: 10.1103/PhysRevC.37.595.

[21] S. Amaducci et al. "Measurement of the ^{140}Ce(n,) Cross Section at n_TOF and Its Astrophysical Implications for the Chemical Evolution of the Universe". In: *Physical Review Letters* 132 (12 Mar. 2024), p. 122701. ISSN: 0031-9007. DOI: 10.1103/PhysRevLett.132.122701.

[22] C. Domingo-Pardo et al. "Advances and new ideas for neutron-capture astrophysics experiments at CERN n_TOF". In: *The European Physical Journal A* 59 (1 Jan. 2023), p. 8. ISSN: 1434-601X. DOI: 10.1140/epja/s10050-022-00876-7. URL: https://link.springer.com/article/10.1140/epja/s10050-022-00876-7.

[23] N. Patronis et al. "The CERN n TOF NEAR station for astrophysics- and application-related neutron activation measurements". In: (Sept. 2022).

[24] G. HEVESY and HILDE LEVI. "Action of Slow Neutrons on Rare Earth Elements". In: *Nature* 137 (3457 Feb. 1936), pp. 185–185. ISSN: 0028-0836. DOI: 10.1038/137185a0.

[25] Nicholas Tsoulfanidis and Sheldon Landsberger. *Measurement Detection of Radiation*. 4th. Taylor Francis, 2015.

[26] A. Gawlik-Ramiega et al. "Measurement of the ^{76}Ge(n,) Cross Section at the n_TOF Facility at CERN". In: *Physical Review C* 104 (4 Oct. 2021), p. 044610. ISSN: 2469-9985. DOI: 10.1103/PhysRevC.104.044610.

[27] G. Tagliente et al. "Neutron Capture on ^{94}Zr: Resonance Parameters and Maxwellian-Averaged Cross Sections". In: *Physical Review C* 84 (1 July 2011), p. 015801. ISSN: 0556-2813. DOI: 10.1103/PhysRevC.84.015801.

[28] C. Lederer et al. "^{197}Au(n,) Cross Section in the Unresolved Resonance Region". In: *Physical Review C* 83 (3 Mar. 2011), p. 034608. ISSN: 0556-2813. DOI: 10.1103/PhysRevC.83.034608.

[29] C. Massimi et al. "^{197}Au(n,) Cross Section in the Resonance Region". In: *Physical Review C* 81 (4 Apr. 2010), p. 044616. ISSN: 0556-2813. DOI: 10.1103/PhysRevC.81.044616.

[30] A.J. Koning et al. "TENDL: Complete Nuclear Data Library for Innovative Nuclear Science and Technology". In: *Nuclear Data Sheets* 155 (Jan. 2019), pp. 1–55. ISSN: 00903752. DOI: 10.1016/j.nds.2019.01.002.

[31] Balraj Singh and Ninel Nica. In: *Nuclear Data Sheets* 113 (2012), p. 1115.

[32] S. K. Basu, G. Mukherjee, and A. A. Sonzogni. In: *Nuclear Data Sheets* 111 (2010), p. 2555.

[33] N. Nica. In: *Nuclear Data Sheets* 187 (2023), p. 1.

[34] Huang Xiaolong and Kang Mengxiao. In: *Nuclear Data Sheets* 133 (2016), p. 221.

[35] Carlo Rubbia. *A HIGH RESOLUTION SPALLATION DRIVEN FACILITY AT THE CERN-PS TO MEASURE NEUTRON CROSS SECTIONS IN THE INTERVAL FROM 1 eV TO 250 MeV: A RELATIVE PERFORMANCE ASSESSMENT*. 1998.

[36] E. Berthoumieux. *The neutron Time-Of-Flight facility, n_TOF, at CERN (I): Technical Description*. 2013.

[37] Enrico Chiaveri and the n_TOF collaboration. *Proposal for n_TOF Experimental Area 2*. 2012.

[38] The n_TOF Collaboration. "The new n_TOF NEAR Station". In: (2020).

[39] U. Abbondanno et al. "Neutron Capture Cross Section Measurement of ^{151}Sm at the CERN Neutron Time of Flight Facility (n_TOF)". In: *Physical Review Letters* 93 (16 Oct. 2004), p. 161103. ISSN: 0031-9007. DOI: 10.1103/PhysRevLett.93.161103.

[40] C. Lederer et al. "Neutron Capture Cross Section of Unstable ^{63}Ni: Implications for Stellar Nucleosynthesis". In: *Physical Review Letters* 110 (2 Jan. 2013), p. 022501. ISSN: 0031-9007. DOI: 10.1103/PhysRevLett.110.022501.

[41] N. Colonna et al. "The fission experimental programme at the CERN n_TOF facility: status and perspectives". In: *The European Physical Journal A* 56 (2 Feb. 2020), p. 48. ISSN: 1434-6001. DOI: 10.1140/epja/s10050-020-00037-8.

[42] J. Praena et al. "Measurement and Resonance Analysis of the ^{33}S(n,)^{30}Si Cross Section at the CERN n_TOF Facility in the Energy Region from 10 to 300 keV". In: *Physical Review C* 97 (6 June 2018), p. 064603. ISSN: 2469-9985. DOI: 10.1103/PhysRevC.97.064603.

[43] Raffaele Esposito and Marco Calviani. "Design of the third-generation neutron spallation target for the CERN's n_TOF facility". In: *Journal of Neutron Research* 22 (2-3 Oct. 2020), pp. 221–231. ISSN: 14772655. DOI: 10.3233/JNR-190137.

[44] C. Weiß et al. "The new vertical neutron beam line at the CERN n_TOF facility design and outlook on the performance". In: *Nuclear Instruments and Methods in Physics Research Section A: Accelerators, Spectrometers, Detectors and Associated Equipment* 799 (Nov. 2015), pp. 90–98. ISSN: 01689002. DOI: 10.1016/j.nima.2015.07.027. URL: https://linkinghub.elsevier.com/retrieve/pii/S0168900215008566.

[45] C. Guerrero et al. "Performance of the neutron time-of-flight facility n_TOF at CERN". In: *The European Physical Journal A* 49 (2 Feb. 2013), p. 27. ISSN: 1434-6001. DOI: 10.1140/epja/i2013-13027-6.

[46] M. Barbagallo et al. "High-accuracy determination of the neutron flux at n_TOF". In: *The European Physical Journal A* 49 (12 Dec. 2013), p. 156. ISSN: 1434-6001. DOI: 10.1140/epja/i2013-13156-x.

[47] M. Sabaté-Gilarte et al. "High-accuracy determination of the neutron flux in the new experimental area n_TOF-EAR2 at CERN". In: *The European Physical Journal A* 53 (10 Oct. 2017), p. 210. ISSN: 1434-6001. DOI: 10.1140/epja/i2017-12392-4.

[48] M. Ferrari et al. "Design development and implementation of the NEAR area and its neutron irradiation station at the n_TOF facility at CERN". In: (Feb. 2022).

[49] C. Ahdida et al. "New Capabilities of the FLUKA Multi-Purpose Code". In: *Frontiers in Physics* 9 (Jan. 2022). ISSN: 2296-424X. DOI: 10.3389/fphy.2021.788253.

[50] Giuseppe Battistoni et al. "Overview of the FLUKA code". In: *Annals of Nuclear Energy* 82 (Aug. 2015), pp. 10–18. ISSN: 03064549. DOI: 10.1016/j.anucene.2014.11.007.

[51] S Goula et al. "NEAR at n_TOF/CERN: Preparing the first multi-foil activation measurement". In: *Adv. Nucl. Phys.* 28 (2022), pp. 117–122. DOI: 10.12681/hnps.3611. URL: https://cds.cern.ch/record/2861079.

[52] S. Goula. *Characterization of the neutron beam at NEAR Station at nTOF/CERN*. 2022.

[53] Davide Chiesa et al. "Measurement of the neutron flux at spallation sources using multi-foil activation". In: *Nuclear Instruments and Methods in Physics Research Section A: Accelerators, Spectrometers, Detectors and Associated Equipment* 902 (Sept. 2018), pp. 14–24. ISSN: 01689002. DOI: 10.1016/j.nima.2018.06.016.

[54] Davide Chiesa, Ezio Previtali, and Monica Sisti. "Bayesian statistics applied to neutron activation data for reactor flux spectrum analysis". In: *Annals of Nuclear Energy* 70 (Aug. 2014), pp. 157–168. ISSN: 03064549. DOI: 10.1016/j.anucene.2014.02.012.

[55] M. E. Stamati. *Feasibility study for neutron inelastic cross section measurements at n_TOF/CERN using HPGe detectors*. 2020.

[56] S. Agostinelli et al. "Geant4—a simulation toolkit". In: *Nuclear Instruments and Methods in Physics Research Section A: Accelerators, Spectrometers, Detectors and Associated Equipment* 506 (3 July 2003), pp. 250–303. ISSN: 01689002. DOI: 10.1016/S0168-9002(03)01368-8.

[57] J. Allison et al. "Geant4 developments and applications". In: *IEEE Transactions on Nuclear Science* 53 (1 Feb. 2006), pp. 270–278. ISSN: 0018-9499. DOI: 10.1109/TNS.2006.869826.

[58] J. Allison et al. "Recent developments in Geant4". In: *Nuclear Instruments and Methods in Physics Research Section A: Accelerators, Spectrometers, Detectors and Associated Equipment* 835 (Nov. 2016), pp. 186–225. ISSN: 01689002. DOI: 10.1016/j.nima.2016.06.125.

[59] D.A. Brown et al. "ENDF/B-VIII.0: The 8 th Major Release of the Nuclear Reaction Data Library with CIELO-project Cross Sections, New Standards and Thermal Scattering Data". In: *Nuclear Data Sheets* 148 (Feb. 2018), pp. 1–142. ISSN: 00903752. DOI: 10.1016/j.nds.2018.02.001.

[60] Sebastian Urlass et al. "Gating of charge sensitive preamplifiers for the use at pulsed radiation sources". In: *Nuclear Instruments and Methods in Physics Research Section A: Accelerators, Spectrometers, Detectors and Associated Equipment* 1002 (June 2021), p. 165297. ISSN: 01689002. DOI: 10.1016/j.nima.2021.165297.

[61] URL: https://www.mirion.com/products/technologies/spectroscopy-scientific-analysis/gamma-spectroscopy/detectors/hpge-shields-accessories/747-747e-lead-shield.

[62] Chhavi Agarwal et al. "Full energy peak efficiency calibration of HPGe detector for point and extended sources using Monte Carlo code". In: *Journal of Radioanalytical and Nuclear Chemistry* 287 (3 Mar. 2011), pp. 701–708. ISSN: 0236-5731. DOI: 10.1007/s10967-010-0820-1.

[63] Jonas Boson, Göran Ågren, and Lennart Johansson. "A detailed investigation of HPGe detector response for improved Monte Carlo efficiency calculations". In: *Nuclear Instruments and Methods in Physics Research Section A: Accelerators, Spectrometers, Detectors and Associated Equipment* 587 (2-3 Mar. 2008), pp. 304–314. ISSN: 01689002. DOI: 10.1016/j.nima.2008.01.062.

[64] N.Q. Huy, D.Q. Binh, and V.X. An. "Study on the increase of inactive germanium layer in a high-purity germanium detector after a long time operation applying MCNP code". In: *Nuclear Instruments and Methods in Physics Research Section A: Accelerators, Spectrometers, Detectors and Associated Equipment* 573 (3 Apr. 2007), pp. 384–388. ISSN: 01689002. DOI: 10.1016/j.nima.2006.12.048.

[65] S. Hurtado, M. García-León, and R. García-Tenorio. "GEANT4 code for simulation of a germanium gamma-ray detector and its application to efficiency calibration". In: *Nuclear Instruments and Methods in Physics Research Section A: Accelerators, Spectrometers, Detectors and Associated Equipment* 518 (3 Feb. 2004), pp. 764–774. ISSN: 01689002. DOI: 10.1016/j.nima.2003.09.057.

[66] Le Thi Ngoc Trang, Huynh Dinh Chuong, and Tran Thien Thanh. "Optimization of p-type HPGe detector model using Monte Carlo simulation". In: *Journal of Radioanalytical and Nuclear Chemistry* 327 (1 Jan. 2021), pp. 287–297. ISSN: 0236-5731. DOI: 10.1007/s10967-020-07473-2.

[67] Joel Gasparro et al. "Monte Carlo modelling of germanium crystals that are tilted and have rounded front edges". In: *Nuclear Instruments and Methods in Physics Research Section A: Accelerators, Spectrometers, Detectors and Associated Equipment* 594 (2 Sept. 2008), pp. 196–201. ISSN: 01689002. DOI: 10.1016/j.nima.2008.06.022.

[68] The n_TOF Collaboration. "Neutron capture cross section measurements by the activation method at the n_TOF NEAR Station". In: (2022).